Viral protein engagement of GBF1 induces host cell vulnerability through synthetic lethality

Running title: Synthetic lethal targeting of a viral-induced hypomorph

Arti T Navare[1], Fred D Mast[1], Jean Paul Olivier[1], Thierry Bertomeu[2], Maxwell Neal[1], Lindsay N Carpp[3], Alexis Kaushansky[1,4], Jasmin Coulombe-Huntington[2], Mike Tyers[2] and John D Aitchison[1,4,5]

1. Center for Global Infectious Disease Research, Seattle Children's Research Institute, Seattle, Washington, USA
2. Institute for Research in Immunology and Cancer, Université de Montréal, Montreal, Quebec, Canada
3. Center for Infectious Disease Research, Seattle, Washington, USA
4. Department of Pediatrics, University of Washington, Seattle, Washington, USA
5. Department of Biochemistry, University of Washington, Seattle, Washington, USA

Correspondence to: John D Aitchison, PhD
Professor and Co-Director
Center for Global Infectious Disease Research
Seattle Children's Research Institute
307 Westlake Avenue North, Suite 500
Seattle Washington, 98109-5219
206-884-3125 OFFICE
john.aitchison@seattlechildrens.org

Character count without spaces: 19,391 (no more than 20,000 characters – not including spaces, methods, or references)

Keywords: synthetic lethality, viral-induced hypomorph, GBF1, genetic interactions, poliovirus

Summary: Using a viral-induced hypomorph of GBF1, Navare et al., demonstrate that the principle of synthetic lethality is a mechanism to selectively kill virus-infected cells.

Abstract

Viruses co-opt host proteins to carry out their lifecycle. Repurposed host proteins may thus become functionally compromised; a situation analogous to a loss-of-function mutation. We term such host proteins viral-induced hypomorphs. Cells bearing cancer driver loss-of-function mutations have successfully been targeted with drugs perturbing proteins encoded by the synthetic lethal partners of cancer-specific mutations. Synthetic lethal interactions of viral-induced hypomorphs have the potential to be similarly targeted for the development of host-based antiviral therapeutics. Here, we use GBF1, which supports the infection of many RNA viruses, as a proof-of-concept. GBF1 becomes a hypomorph upon interaction with the poliovirus protein 3A. Screening for synthetic lethal partners of GBF1 revealed ARF1 as the top hit, disruption of which, selectively killed cells that synthesize poliovirus 3A. Thus, viral protein interactions can induce hypomorphs that render host cells vulnerable to perturbations that leave uninfected cells intact. Exploiting viral-induced vulnerabilities could lead to broad-spectrum antivirals for many viruses, including SARS-CoV-2.

Introduction

RNA viruses are prevalent and pervasive pathogens responsible for many global health crises, including the COVID-19 pandemic (Carrasco-Hernandez et al., 2017; Enard and Petrov, 2020; Rosenberg, 2015; Woolhouse and Gaunt, 2007). RNA viruses typically have high mutation rates enabling them to rapidly adapt to new cell types, infect new host species, evade host immune responses, and quickly develop antiviral drug resistance (Sanjuán et al., 2010). Currently, the repertoire of U.S. Food and Drug Administration approved antivirals is limited, targeting only eight out of the known 214 human-infecting RNA viruses (Heaton, 2019). Almost exclusively, these U.S. Food and Drug Administration approved drugs are all designed to target viral proteins (Heaton, 2019; Woolhouse and Brierley, 2018). The dearth of antivirals is likely impacted by the many challenges faced in antiviral drug development, including the small list of target viral proteins

52 due to their compact genomes, the quick emergence of escape mutants due to the high mutation
53 rates prevalent in many RNA viruses, and the limited therapeutic range of antivirals due to the
54 diversity of RNA virus serotypes which, akin to antimicrobial resistance, has led to limited strain-
55 specific use, or even discontinuation of use, for many antivirals (Heaton, 2019; Irwin et al., 2016;
56 Pennings, 2013; van der Vries et al., 2013). Yet, the same compact-sized genome that gives
57 these viruses an edge over antivirals also makes them obligatory pathogens that rely on host
58 proteins for survival. Thus, although viral genomes drift, they often maintain reliance on the same
59 subset of host factors (Gordon et al., 2020a; Heaton, 2019). The idea of exploiting this over-
60 reliance on their host to develop host-directed antivirals to interfere with host cell factors that are
61 required by the virus, or to more broadly influence immune responses is gaining traction (Gordon
62 et al., 2020b; Kaufmann et al., 2018; Mast et al., 2020; Prussia et al., 2011).

63 Host-based therapies expand opportunities for treating viral infections (Brass et al., 2008;
64 Krishnan and Garcia-Blanco, 2014; Zhou et al., 2008). To proliferate, viruses must co-opt
65 common host pathways and cellular machineries by forming protein-protein interactions with host
66 proteins (Basler et al., 2019; Carpp et al., 2014; Gordon et al., 2020b; Lum and Cristea, 2016;
67 Saeed et al., 2020; Stukalov et al., 2020). Due to the essential requirement of these interactions,
68 they are likely to be conserved within viral lineages and can be targeted for developing broad-
69 spectrum therapeutics (de Chassey et al., 2014; Meyniel-Schicklin et al., 2012; Pfefferle et al.,
70 2011). Recently, an analysis of published virus-host interaction datasets revealed RNA viruses
71 frequently engage so-called “multifunctional host proteins”, a set of 282 highly connected proteins
72 as assessed by their protein-protein interaction networks (Heaton, 2019; Navratil et al., 2009).
73 Targeting these multifunctional host proteins with drugs, many approved by the U.S. Food and
74 Drug Administration could disrupt several crucial steps of viral replication. Inhibiting a virus by
75 targeting the host reduces the possibility of drug resistance and is potentially broad-spectrum if
76 more than one virus relies on the same host protein. However, inhibiting these multifunctional

77 proteins by drugs may also elicit adverse effects on the host because often these proteins tend
78 to be essential and serve as hubs of complex protein interaction networks (Heaton, 2019; Zotenko
79 et al., 2008). Thus, host-based therapeutic targets should be chosen carefully to avoid potential
80 serious adverse side effects and, ideally, strategies that selectively affect only infected cells
81 should be sought.

82 The principle of synthetic lethality offers an opportunity for selectively targeting virus
83 infected cells by drugging synthetic lethal (SL) interactors of virus-targeted multifunctional protein
84 hubs (Mast et al., 2020). Synthetic lethality occurs between two genes when a loss-of-function
85 mutation in either gene has little impact on cell viability, but becomes detrimental when paired
86 together resulting in cell death (Dobzhansky, 1946; Hartwell et al., 1997) (Fig. 1A). Such lethal
87 genetic combinations, known as “synthetic lethal pairs” (Nijman, 2011a), are one of many forms
88 of genetic interactions that can occur within cells (Boone et al., 2007; Dixon et al., 2009; Drees et
89 al., 2005; Horlbeck et al., 2018). The existence of synthetic lethality reveals important aspects of
90 the genetic architecture of cells, demonstrating the presence of genetic buffering in organisms
91 due to functional redundancy (Horlbeck et al., 2018; McManus et al., 2009). This SL concept has
92 been successfully applied to cancer therapy and host-targeted drug development (Farmer et al.,
93 2005; Kaelin, 2005; Mendes-Pereira et al., 2009; Turner et al., 2008; Wiltshire et al., 2010) (Fig.
94 1B). For example, loss-of-function mutations in the DNA repair genes encoded by breast cancer
95 type 1 and 2, *BRCA1* and *BRCA2,* cause breast and ovarian cancer but exhibit enhanced
96 sensitivity to inhibitors of poly ADP-ribose polymerase (*PARP*), another DNA repair enzyme
97 (Farmer et al., 2005). PARP inhibitors selectively killed cancerous cells carrying the loss-of-
98 function *BRCA* mutation while sparing noncancerous cells (Bryant et al., 2005) and in a clinical
99 trial, PARP anticancer drugs showed a significantly longer progression-free period in patients with
100 breast cancer (Litton et al., 2018). Synthetic lethality-inspired anticancer therapy provides
101 avenues for improved drug specificity and efficacy at lower doses, thereby limiting side effects

102 (Beijersbergen et al., 2017). Here, we extend the application of this synthetic lethality principle to
103 host-derived antiviral targets.

104 Virus infection is a perturbation of the host protein-protein interaction (PPI) network.
105 Interactions between virus and host proteins usurp normal protein functions and rewire host PPI
106 networks. Host proteins are considered proviral if loss of function renders the host cell resistant
107 to infection, and antiviral if loss of function improves cell permissibility to infection. Infected cells
108 exhibit altered metabolic requirements (Thaker et al., 2019), signaling pathways (Gaur et al.,
109 2011), intracellular transport pathways (Belov et al., 2007) and other morphological and molecular
110 characteristics relative to the noninfected cells. In such situations, infected cells may depend on
111 a different complement of proteins than their uninfected counterparts (Mast et al., 2020). This
112 state-specific vulnerability may be a target for host-based therapeutics based on the well-
113 established principle of synthetic lethality. For example, if two host cell proteins have a SL
114 relationship and the function of one protein is hijacked by a viral protein, then cells may become
115 dependent on the function of the second protein. In contrast, cells that are not altered by the virus,
116 i.e., those that are uninfected, will be unimpacted by blocking the second protein, since the
117 elimination of a single half of the SL pair does not result in a phenotype. Rational targeting of SL
118 protein pairs in which the function of one partner is reduced specifically in the infected cell; a
119 situation equivalent to the mutant gene in cancer, is a novel framework for taking advantage of
120 the intrinsic differences of infected cells to achieve selective targeting (Fig. 1C). We hypothesize
121 that viral-host PPIs generate protein-based, viral-induced (vi)-hypomorphs of host factors in
122 infected cells, thereby specifically sensitizing infected cells to targeting SL/synthetic sick partners
123 of these vi-hypomorphs. To test this hypothesis, we selected the Golgi-specific brefeldin A-
124 resistance guanine nucleotide exchange factor (GBF1) (Claude et al., 1999) because it is a critical
125 proviral host factor for the replication of several families of RNA viruses, including *Picornaviridae,*
126 *Coronaviridae, Flaviviridae*, *Herpesviridae*, *Filoviridae*, and *Rioviridae* (Belov et al., 2008b; Carpp

127 et al., 2014; Farhat et al., 2018; Goueslain et al., 2010; Lanke et al., 2009; Martínez et al., 2019;
128 Verheije et al., 2008; Yamayoshi et al., 2010). Considering so many viruses rely on GBF1, it
129 seems unlikely that these viruses would readily overcome GBF1 dependence. GBF1 mediates
130 recruitment of coat proteins (Manolea et al., 2008), lipid modifying enzymes (Ellong et al., 2011),
131 and protein tethers (García-Mata and Sztul, 2003) to Golgi membranes. It thus plays a central
132 role in vesicular transport through the Golgi, the structural integrity of Golgi membranes, and the
133 maintenance of lipid homeostasis (Beller et al., 2008; Donaldson and Jackson, 2011; Guo et al.,
134 2008; Sáenz et al., 2009; Soni et al., 2009). With its dynamic membrane-modulating functions
135 GBF1 has also been implicated in coatomer-dependent protein delivery to lipid droplets
136 (Kaczmarek et al., 2017; Soni et al., 2009).

137 Many RNA viruses encode proteins that bind GBF1 directly, including the nonstructural
138 proteins 3A of poliovirus (Belov et al., 2008a; Teterina et al., 2011) and coxsackievirus (Wessels
139 et al., 2006a; c), and nonstructural protein 5 of dengue (Carpp et al., 2014). Recently, two SARS-
140 CoV-2 proteins, membrane (M) and orf6, were identified to be directly binding or in close proximity
141 of GBF1, respectively (Laurent et al., 2020; Stukalov et al., 2020). In the case of poliovirus
142 infection, 3A redistributes GBF1 to viral replication complexes during early stages of replication
143 and subverts its guanine nucleotide exchange factor (GEF) function in the infected cells (Carpp
144 et al., 2014; Richards et al., 2014; Wessels et al., 2007, 2006b; c), suggesting that poliovirus
145 protein 3A may attenuate GBF1's normal function creating a hypomorph, rendering cells
146 susceptible to disruption of proteins synthetically lethal with *GBF1*. Here, we provide proof-of-
147 concept that SL partners of vi-hypomorphs can be targeted to selectively eliminate infected cells
148 while leaving uninfected cells intact. We do this by performing a genome-wide chemogenomic
149 CRISPR screen to identify SL partners of *GBF1*, validating the top candidates, and demonstrating
150 that shRNA-mediated silencing of the *GBF1* SL interacting partner, *ARF1*, selectively kills cells
151 expressing poliovirus protein 3A.

152 **Results and Discussion:**

153 In order to identify putative synthetic lethal partners of *GBF1*, we screened a high-complexity
154 extended-knockout CRISPR library of 278K single guide RNAs (sgRNAs) that target 19,084
155 RefSeq genes, 20,852 alternatively-spliced genes, and 3,872 predicted genes, among additional
156 controls, in NALM-6 human B cell precursor leukemia cells (Bertomeu et al., 2018) (Fig. 2A).
157 These cells harbor a genomic doxycycline-inducible Cas9 that enables regulatable, uniform, and
158 robust gene silencing across the pooled library (Wang et al., 2014). Relative changes in sgRNA
159 frequencies were obtained from sequencing populations of the CRISPR libraries cultured in the
160 presence or absence of Golgicide A (GCA), a potent and specific inhibitor of the GEF activity of
161 GBF1 (Sáenz et al., 2009) (Fig. 2A). The concentration of 4 μM GCA used in the screen was
162 determined prior to the screen to maximize both enrichment, i.e., positive selection for rescue of
163 compound toxicity, and depletion, i.e., negative selection for SL interactions (Fig. S1). sgRNA
164 frequencies were determined by sequencing, and relative fold changes in sgRNA abundances
165 between GCA- and mock-treated samples were reported (Table S1 and Fig. 2B).

166 Using an FDR cutoff of <0.05, there were 53 underrepresented genes and 17
167 overrepresented genes in the GCA treated samples relative to the controls (Fig. 2B; white circles).
168 Underrepresented genes represent putative SL partners of GBF1 and the top SL candidate, ADP-
169 ribosylation factor 1 (ARF1), is a small GTPase that regulates the recruitment and assembly of
170 COP I on Golgi and ERGIC membranes (Liang and Kornfeld, 1997). GBF1 facilitates GDP to GTP
171 exchange on ARF1 to regulate recruitment of effectors such as coat protein and lipid-modifying
172 enzymes to ARF1-localized membrane sites and creates a domain competent for secretory cargo
173 transport (Claude et al., 1999; Donaldson and Jackson, 2011; Kawamoto et al., 2002). In yeast,
174 a negative genetic interaction exists between *ARF1* and the yeast GBF1-ortholog, guanine
175 nucleotide exchange on ARF 1 (*GEA1*) (Surma et al., 2013), and *GEA1* overexpression rescues
176 an *arf1*Δ temperature sensitive growth defect (Chantalat et al., 2003). Functional enrichment

177 analysis of the 53 putative SLs of GBF1 showed enrichment for genes in the early secretory
178 pathway, and genes involved in the misfolded protein-triggered ER stress response (Fig. 2C, D).
179 *GBF1* depletion is known to induce an unfolded protein response in the ER (Citterio et al., 2008).
180 Thus, putative SLs of GBF1 are likely functionally redundant with GBF1, an attribute of the genetic
181 interactions between SLs that offers buffering in the event of a loss of function of one of the SL
182 genes (Hartman IV et al., 2001; Mast et al., 2020). As evident by a PPI network, the 53 *GBF1*-
183 SLs and the 17 *GBF1* suppressors are functionally related and can be grouped into a few distinct
184 functional clusters (Fig. 2D). For example, one cluster of *GBF1*-SLs are enriched in ER stress,
185 unfolded protein response, and ER-associated protein degradation pathways, while eight out of
186 the seventeen *GBF1* suppressors contribute to ER-Golgi vesicular transport (Fig. 2D). GBF1-SLs
187 also include a cluster of RNA binding proteins, and members of the KICSTOR (Wolfson et al.,
188 2017) and DEPTOR (Peterson et al., 2009) complexes that negatively regulate mTOR signaling
189 (Fig. 2D). Several genes from both lists possess GTPase activity, e.g., the *GBF1*-SLs: *ARF1*,
190 *TMED10*, *DRG2*, *RAB5C*, *YIP5*, *RAB3GAP2*, and the *GBF1* suppressors: *ARF1GAP1*, *SAR1A1*,
191 *ARF4*, and *ARF5* (Fig. 2D). ARF4, a class II ARF implicated in endosomal morphology and
192 retrograde transport to the Golgi (Nakai et al., 2013), was the top overrepresented gene (Fig. 2B).
193 A previous large-scale insertion mutagenesis screen identified a role for ARF4 in conferring
194 resistance to Golgi disrupting agents (Reiling et al., 2013), suggesting a protective role of ARF4
195 against GCA toxicity. Just over half of the GBF1-SLs and suppressors identified in our screen are
196 directly targeted by viral proteins (Fig. 2D, circles with red boundaries).

197 We searched this list against the Drug Gene Interaction Database (Cotto et al., 2018) for
198 potential 'druggability' (http://dgidb.org/search_categories) and selected four druggable, putative
199 synthetic lethal interactors of *GBF1* (Fig. 2A). In addition to *ARF1*, we selected: heat-shock protein
200 90 (*HSP90*), a protein chaperone with ATPase activity (Rowlands et al., 2010); C-terminal Src
201 kinase (*CSK*), which negatively regulates Src family kinases and has roles in cell growth,

202 differentiation, migration and immune response (Okada, 2012); and protein kinase, AMP-
203 activated, alpha 1 (*PRKAA1*), the catalytic subunit of the 5'-prime-AMP-activated protein kinase
204 (AMPK) with roles in regulating cell stress and metabolism (Sanli et al., 2014). These four putative
205 SL partners of GBF1 were silenced in HeLa cells along with methylsterol monooxygenase 1
206 (*MSMO1*), included as a control because it did not show depletion or enrichment in sgRNA
207 abundance, and *ARF4*, because it was the topmost significantly overrepresented in our drug
208 CRISPR screen (Table S1 and Fig. 2A). The knockdown (KD) cell lines were incubated with 1.5
209 μM or 4 μM of GCA/DMSO-alone for 48 h before measuring viabilities. Synthetic lethal effects of
210 combining GCA with shRNA-mediated depletion were observed in *ARF1* KD cells with only 40%
211 or 50% viability as compared to the DMSO-treated cells at 4 μM and 1.5 μM GCA concentration,
212 respectively (Fig. 3A). When the viability of each KD cell line was compared to that of the *MSMO1*
213 KD control, the decrease in the viability was statistically significant for *ARF1* KD at both
214 concentrations, confirming the results of the chemogenomic screen. A GCA dose-response assay
215 monitoring cell growth inhibition as a function of GCA concentration showed a nearly two-fold
216 reduction in IC_{50} value for *ARF1* KD cells as compared to the control (Fig. 3B), further validating
217 the SL interaction between *GBF1* and *ARF1*.

218 The premise of SL-driven antivirals is that a viral infection disrupts normal protein functions
219 consequently generating vi-hypomorphs in infected cells. As a result, the infected cells may
220 become more vulnerable to drugs that target SL partners of the vi-hypomorph than in uninfected
221 cells lacking the vi-hypomorph. We tested this hypothesis in the context of expressing poliovirus
222 3A because it recruits GBF1 to sites of poliovirus replication (Belov et al., 2007, 2008a; Richards
223 et al., 2014). The dynamics of GBF1-3A interactions observed during viral infection, including
224 GBF1-mediated ARF1 activation and translocation, are retained in cells ectopically expressing
225 the viral protein alone (Belov et al., 2005, 2007; Richards et al., 2014; Wessels et al., 2006a),
226 which allows for testing the formation of a GBF1 vi-hypomorph in a simpler yet relevant model

227 system without the confounding effects of viral infection. We tagged poliovirus protein 3A with a
228 modified FLAG epitope (FLAG*) (Teterina et al., 2011) and transiently expressed it in HeLa cells
229 (Fig. 4). Poliovirus isolates expressing a modified FLAG tagged 3A are stable and yielded 3A-
230 tagged viruses with similar fitness to the wild-type untagged virus, suggesting that this protein
231 behaves in a similar manner as the wildtype protein (Teterina et al., 2011). The FLAG* tag is
232 similar to the conventional 8-amino acid (DYKDDDDK) FLAG tag, but with the last aspartic acid
233 replaced by tyrosine and is recognized by α-FLAG antibodies (Teterina et al., 2011) (Fig. 4A). N-
234 terminal, FLAG*-tagged 3A, or an empty plasmid control was transiently transfected into HeLa
235 cells for 24 h. 3A-FLAG* and associated proteins were affinity purified on magnetic beads
236 conjugated with α-FLAG antibodies (Fig. 4A). Isolated complexes were washed, and the eluate,
237 along with a fraction of the load and wash were resolved by SDS-PAGE, transferred to
238 nitrocellulose, and probed with α-FLAG and α-GBF1 antibodies (Fig. 4A). A band of ~10 kDa was
239 detected in the eluate corresponding to the FLAG*-3A protein and a slower migrating, high
240 molecular weight band of ~200 kDa, corresponding to GBF1, was detected in the eluate of GBF1
241 immunoprecipitated from cell expressing 3A-FLAG*, but not from cells transfected with the empty
242 plasmid control (Fig. 4A). This observation confirmed that the ectopically expressed 3A-FLAG*
243 protein retained its ability to physically interact with GBF1, as reported previously (Teterina et al.,
244 2011).

245 We next tested if the physical interaction between 3A and GBF1 had consequences for
246 GBF1 function, suggestive of a GBF1 hypomorph. HeLa cells were transduced with lentivirus
247 delivering an empty control or 3A-FLAG*and cells were fixed and immunostained with α-FLAG-
248 647 (red) and α-GBF1-488 (green), antibodies (Fig. 4B). GBF1 was visualized as puncta enriched
249 in a juxtanuclear position consistent with a Golgi localization in the control cells (Fig. 4B; red
250 arrows). This juxtanuclear enrichment was lost in 3A transduced cells and the GBF1 puncta were
251 instead found redistributed throughout the cytoplasm (Fig. 4B). We quantified this redistribution

252 by measuring the distance of all GBF1 puncta from the nearest nucleus for each cell in the dataset
253 (Fig. 4C, D). This quantification revealed an increase in GBF1 puncta localized away from the
254 nucleus in 3A transduced cells that was statistically significant compared to control. The depletion
255 of Golgi-localized GBF1 upon expression and interaction with poliovirus 3A is consistent with 3A
256 inducing a GBF1-hypomorph.

257 Having identified *ARF1* as a SL interactor of *GBF1* and established that a GBF1
258 hypomorph may be induced by expression of poliovirus 3A, we next asked if the 3A-induced
259 hypomorphic state of GBF1 was sufficient to drive a synthetic lethal interaction in cells depleted
260 of ARF1. HeLa cells were treated with shRNA to *ARF1*, or, as a control, shRNA to *MSMO1*, which
261 had no effect in the *GBF1* SL screen (Fig. 2B), and the depletion of ARF1 was evaluated by
262 western blotting (Fig. S2). 3A-FLAG*or an empty plasmid control was transiently transfected into
263 both KD cell lines and expression of 3A-FLAG* was detected by flow cytometry (Fig. 5A). The
264 viability of the *ARF1* KD cells was significantly decreased by the expression of 3A-FLAG* (Fig.
265 5B). By comparison, the *MSMO1* KD cells were not significantly affected (Fig. 5B). Importantly,
266 this decrease in cell viability, 30% ± 3.5, (Fig. 5B) was comparable to the percent of *ARF1* KD
267 cells expressing 3A-FLAG*, 37% ± 3.0 (Fig. 5A), supporting our hypothesis that the 3A expressing
268 cells in which a hypomorph of GBF1 was generated due to GBF1-3A interaction were selectively
269 killed only in the absence of a functional *ARF1* (Fig. 5).

270 Synthetic lethality is conventionally described as a type of genetic interaction between two
271 nonessential genes that participate in a parallel or redundant process to carry out an essential
272 function, where mutations in either gene alone does not affect cell viability, but mutations in both
273 genes results in cell death (Nijman, 2011b). In this manuscript, we have extended the idea of
274 synthetic lethality to interactions involving a virus-induced hypomorph. In poliovirus, the viral
275 replication complex protein 3A physically interacts with GBF1 (Belov et al., 2008a; Teterina et al.,

276 2011) and re-localizes it to poliovirus replication complexes (Richards et al., 2014). We show
277 here, that this re-localization sensitizes and reduces the viability of cells depleted of ARF1.

278 In summary, viral-host protein-protein interactions that result in the functional attenuation
279 of the host factor offer a promising avenue for therapeutics based on the principle of synthetic
280 lethality (Mast et al. 2020). In this context, the infected cell becomes selectively dependent upon
281 the otherwise nonessential SL partner of the vi-induced hypomorph. Considering that GBF1 is a
282 common target of many viruses, it is tempting to speculate that SL interactors of *GBF1*, or other
283 common proviral factors, might be candidates for broad-spectrum host-based antivirals. Our
284 proof-of-concept experiments provide a rational approach for identifying these novel antivirals.
285 Our strategy to target SL interactions of the vi-induced hypomorph has a potential to change the
286 current paradigm for host-based therapeutics that can lead to broad spectrum antivirals and can
287 be applied to other intracellular pathogens.

288 ## Materials and Methods

289 ### Cell culture and plasmids

290 HeLa cells (ATCC CCL-2) and HEK293-FT (ThermoFisher) were cultured at 37 °C in 5% CO_2 in
291 medium composed of high glucose Dulbecco's modified eagles medium (DMEM, Gibco)
292 supplemented with 10% (v/v) heat inactivated fetal bovine serum (VWR), 1×
293 penicillin/streptomycin (ThermoFisher Scientific), 20 mM L-glutamine (Gibco), 1× nonessential
294 amino acids (Gibco), 1× sodium pyruvate (Gibco) and 10 mM HEPES buffer (Gibco) (complete
295 media).

296 Cell line authentication was provided by the American Type Culture Collection and
297 ThermoFisher Scientific. In general, cells were passaged 5-10 times and periodically tested for
298 contamination using MycoAlert™ Mycoplasma Detection (Lonza) kit.

299 A doxycycline-inducible Cas9 clonal cell line of NALM-6 cells (Wang et al., 2009) was
300 cultured at 37 °C in 5% CO2 in RPMI-1640 medium supplemented with 10 % (v/v) heat inactivated
301 fetal bovine serum, as described (Bertomeu et al., 2017).

302 Agarose stabs of *E. coli* (DH10B) harboring custom-made mammalian expression vector pD2109-
303 EF1 was purchased from ATUM (Newark, CA USA). pD2109-EF1 encodes poliovirus protein 3A
304 with a modified FLAG tag (DYKDDDYK) inserted at the N-terminus. The modified FLAG tag
305 (referred here as FLAG*), contains a tyrosine (Y) residue at position 7 instead of aspartic acid
306 residue (D) found in a typical FLAG tag sequence. A complete sequence of the 3A-FLAG*protein
307 with the inserted FLAG* tag (in bold) is as follows:

308 GPLQYK**DYKDDDYK**DLKIDIKTSPPPECINDLLQAVDSQEVRDYCEKKGWIVNITSQVQTERNIN
309 RAMTILQAVTTFAAVAGVVYVMYKLFAGHQ

310 Plasmid DNA was purified from the agarose stabs using NucleoBond Xtra Midiprep kit
311 (Macherey Nagel) by following manufacture's protocol. 3A-FLAG* protein was expressed in HeLa

312 cells by plasmid DNA transfection. We used an empty plasmid pLKO1.puro with comparable size
313 to pD2109-EF1 as a control for transfections.

314 Bacterial glycerol stocks of MISSION® shRNAs were purchased from Sigma Aldrich for:
315 *ARF1* (clone ID: TRCN0000039874, TRCN0000039875), *ARF4* (TRCN0000298174,
316 TRCN0000047940), *MSMO1* (TRCN0000230198, TRCN0000046245), CSK(TRCN0000199500,
317 TRCN0000000804), *HSP90* (TRCN0000008747,TRCN0000315415), and *PRKAA1*
318 (TRCN0000000861, TRCN0000000859). shRNA plasmid DNA was purified using NucleoBond
319 Xtra Midiprep kit by following manufacture's protocol.

320 **Chemogenomic screening and data analysis**

321 Genome-wide custom extended-knockout (EKO) pooled library was created in a B-cell lymphoma
322 line using a published protocol (Bertomeu et al., 2018). Briefly, a clone of the NALM-6 cells
323 expressing Cas9 under a doxycycline-inducible promoter was transduced with the 278K sgRNAs
324 followed by selection over blasticidin, and induction of knockdown of genes with 2 μg/ml
325 doxycycline over a seven-day period. At that time (day 0), the EKO library was split into separate
326 flasks, one containing 4 μM GCA, three containing media alone and two containing 0.1% DMSO
327 and each library flask was grown for eight more days. During this period, cell counts were made
328 every two days and population doublings were monitored. After each cell count, cells were diluted
329 down to 28 million cells per flask and fresh media was added. Whereas all other samples were
330 grown in T-75 flasks from days 0-8 of the screen, one of the untreated control samples was grown
331 in a T-175 flask and was diluted down to 70 million cells every two days instead of 28 million.
332 sgRNA sequences were recovered by PCR of genomic DNA, reamplified with Illumina adapters,
333 and sequenced on an Illumina HiSeq 2000 instrument. The GCA-treated sample DNA was later
334 re-sequenced on an Illumina Next-Seq 500 instrument to increase coverage. Illumina sequencing
335 reads were aligned to the theoretical EKO library using Bowtie 2.2.5, with the -norc (no reverse
336 complement) option and otherwise default parameters. sgRNA read counts were tabulated from

337 all successfully aligned reads. Having found no significant differences between untreated and
338 0.1% DMSO-treated controls, we opted to add together the sgRNA read counts from all control
339 samples to generate a more robust estimate of the expected sgRNA frequency distribution. We
340 used RANKS (Robust Analytics and Normalization for Knockout Screens) (Bertomeu et al., 2018)
341 with default parameters to generate gene scores p-value and FDR values, comparing the sgRNA
342 read counts of the GCA-treated sample to those of the controls (Table S1). We also calculated
343 gene-level $\log_2$ fold-changes in sgRNA representation by first summing across each sample the
344 reads of all (usually 10) sgRNAs targeting the gene to calculate a single ratio normalized to the
345 ratio of total aligned read counts per sample (Table S1). This approach effectively downweighs
346 less well represented guides in contrast to the traditional approach of taking the average of the
347 individual sgRNA fold-changes. Reported gene essentiality and essentiality rank in Table S1 are
348 from a previous screen (Bertomeu et al., 2018).

349 Ontology biological process enrichment analysis was performed on the putative GBF1-
350 SLs (FDR < 0.05) using ClusterProfiler (Yu et al., 2012) where the list was analyzed against the
351 entire KO genes from the CRISPR library to functionally classify the SL genes.

352 The list of 70 genes (53 GBF1- SLs and 17 GBF1 suppressors) passing the FDR cut off
353 (< 0.05) was submitted to the STRING database (Szklarczyk et al., 2019) to map evidence-based
354 PPIs with the active interaction sources: textmining, experiments, databases, co-expression,
355 neighborhood, gene-fusion, and co-occurrence. The resulting PPI network was visualized using
356 Cytoscape (3.8.2) (Shannon et al., 2003) in a radial layout, with proteins denoted as circles and
357 interactions as edges. The 70 genes were also searched against a virus-host PPI database,
358 VirHostNet (v2.0) (Navratil et al., 2009), to identify known interactors of virus proteins.

359 **10× Lentivirus stock preparation**

360 Glycerol stocks of the validated MISSION shRNA vectors for *ARF1*, *PRKAA1*, *HSP90*, *CSK*,
361 *MSMO1* and *ARF4*, were obtained from Sigma Aldrich (St. Louis, MO). 10× stocks of non-

362 replicating lentiviral stocks were generated by transfection of HEK293-FT cells as follows: 4×10^6
363 HEK293-FT cells were plated on poly-L-lysine coated 10 cm dishes to achieve 70-80% confluency
364 at time of transfection. The following day, transfection mixtures were prepared by mixing 20 µl
365 Polyethylenimine MAX (Polysciences Inc, Warrington, PA) prepared at 1 mg/ml, together with
366 4.75 µg of transgene shRNA constructs, 1.5 µg of viral envelope plasmid (pCMV-VSV-G), and
367 3.75 µg of viral packaging plasmid (psPax2). After incubating for 10 min at room temperature in
368 DMEM, transfection complexes were added dropwise to cells. After overnight incubation, cells
369 were washed to remove the transfection mixture and replaced with 10 ml of pre-warmed media.
370 Lentivirus-containing supernatant was harvested 48 h later, centrifuged for 5 min at 900 *g* to
371 remove cell debris, passed through 0.45 µm syringe filters, and collected by centrifugation for 4 h
372 at 78,900 *g*. Supernatants were decanted and pelleted lentiviruses were re-suspended in 0.1 ml
373 Opti-MEM (Gibco) to obtain 10× lentivirus concentrates and stored at -80 ˚C until use. A similar
374 protocol was used to prepare 10× lentivirus stocks of 3A-FLAG*.

375 **shRNA-mediated gene knockdowns**

376 To induce knockdown of the top putative GBF1 SL genes, 300,000 HeLa cells were transduced
377 with lentiviral supernatants in 6-well plates. At time of plating, 10× lentivirus concentrates were
378 diluted in 1 ml of Opti-MEM containing 8×10^{-3} µg/ml of polybrene (Sigma Aldrich; St. Louis, MO)
379 and incubated overnight at 37 ˚C. The following day, the transfection mix was replaced with 2 ml
380 of pre-warmed complete media and incubated for 24 h. In order to select for cells with stable
381 integration of shRNA transgenes, overnight media was replaced with complete media containing
382 1.5 µg/ml puromycin. Cells were selected for at least 3 days prior to experiments. Stably silenced
383 knockdown cell lines (*ARF1* KD, *HSP90* KD, *CSK* KD, *PRKAA1* KD, *MSMO1* KD, and *ARF4* KD)
384 were harvested by trypsinization in 0.25% trypsin-EDTA, washed in pre-warmed PBS, cells were
385 counted, and a small aliquot was cells were saved for western blot analysis to verify protein level
386 knockdown efficiencies for each gene.

387 **Western blot analysis**

388 Cell pellets of the KD cell lines were re-suspended in a chilled IP lysis buffer (20 mM HEPES-
389 KOH, pH 7.5, 1% (w/v) Triton X-100, 0.5% (w/v) sodium deoxycholate, 110 mM potassium
390 acetate, 2 mM $MgCl_2$, 25 mM NaCl, and 1× cOmplete protease inhibitor cocktail (Roche)) and
391 lysed by sonicating for 1 min using a probe sonicator (QSonica) operated at an amplitude of 10
392 with 10 s on-off cycles. Lysates were centrifuged at ~100,000 *g* for 5 min and supernatants were
393 transferred into a fresh tube. Protein concentrations were determined by bicinchoninic acid assay
394 (ThermoFisher Scientific) and working solutions of lysates at concentrations of 15-30 µg total
395 proteins per 30 µl were prepared with 1× lithium dodecyl sulfate (LDS) sample buffer with reducing
396 reagent (NuPAGE, ThermoFisher Scientific) followed by heating at 70 ˚C for 20 min on a
397 Thermomixer (Eppendorf). 30 µl of the reduced lysate was loaded per well on 4-20% or 12%, for
398 *ARF1* KD and *ARF4* KD, Bis-Tris gels (NuPAGE, ThermoFisher Scientific) and protein bands
399 were resolved at a constant voltage of 170 V for 1 h. Protein bands were transferred on PVDF
400 membranes using Xcell2 blot module (ThermoFisher) for 2 h at a constant voltage of 37 V and
401 membranes were blocked in 5% (w/v) milk in TBST for 1 h at room temperature. After blocking,
402 membranes were incubated with primary antibodies (Abcam and GeneTex) against proteins of
403 interests: ARF1 (ab58578 at 1:1000 dilution), ARF4 (ab190000 at 1:1000 dilution), HSP90
404 (GTX101448 at 1:1000 dilution), CSK (GTX107916 at 1:500 dilution), CSNK2A (13-453 at 1:500
405 dilution), PRKAA1 (ab32047 at 1:1000 dilution) and MSMO1 (ab116650 at 1:500 dilution) and
406 washed thrice in TBST buffer before incubating with appropriate HRP-conjugated secondary
407 antibodies (goat α-mouse or α-rabbit; 1:2500 dilution). Following incubation, membranes were
408 washed and developed using chemiluminescent substrates (Advansta WesterBright). Images
409 were acquired using a FluorChem imager (Protein Simple), and membranes were stripped using
410 a stripping buffer (ThremoFisher), blocked, incubated with HRP-α-β-actin (ab49900; 1:25,000)
411 and imaged as before. Images were cropped, adjusted for brightness and contrast, and labelled
412 using Adobe Photoshop and InDesign.

413 **FLAG*-tagged 3A lentivirus direct plasmid transfection**

414 FLAG*-tagged 3A plasmid DNA were directly transfected in HeLa cells for performing
415 immunofluorescent imaging and co-immunoaffinity purification assays using TransIT transfection
416 reagent (Mirus) by following the manufacturer's recommended protocol. Briefly, transfection mix
417 was prepared in a serum free Opti-MEM media by adding 3A-FLAG* DNA and TransIT reagent
418 in a ratio of 1:3 (wt/v) and the mixture was incubated for 30 min at room temperature. After
419 incubation, the transfection mix volume equivalent to 1 μg and 15 μg total DNA was added to
420 60,000 HeLa cells for immunofluorescence imaging and 3×10^6 cells for co-immunoaffinity
421 purification assays, respectively.

422 **Flow cytometry**

423 Transduced HeLa cells were trypsinized using 0.05% (w/v) Trypsin-EDTA and transferred into a
424 U-bottom 96-well plate. Cells were washed twice in PBS supplemented with 10% (v/v) FBS and
425 incubated with Live/Dead Fixable stain (excitation/emission: 416/451; ThermoFisher Scientific)
426 for 15 min on ice. Excess stain was removed by washing twice and cells were fixed using 4%
427 (w/v) paraformaldehyde (Sigma) for 30 min. Fixative solvent was removed, and cells were washed
428 thrice in PBS by centrifugation at 700 *g* for 5 min. Supernatant wash solution was removed, and
429 cells were incubated in PBS with 0.1% (w/v) Triton X-100 for 15 min to permeabilize the cells.
430 After cell permeabilization, the cells were blocked for 1 h in PBS containing 2% (w/v) BSA
431 (manufacturer) and 1% (w/v) Triton X-100. Cells were then stained with R-phycoerythrin (PE)-
432 conjugated α-FLAG (637310; Biolegends, 1:1000 dilution) for 1 h on ice. After staining, cells were
433 washed thrice in the blocking buffer and analyzed on a LSRII flow cytometer (BD Biosciences).
434 The percentage of cells expressing 3A-FLAG* were determined by analyzing the flow cytometry
435 data using FlowJo software (Tree Star, Inc.). Cell populations were filtered using the forward and
436 side scatter to remove cell debris and cell doublets. The remaining single cell subpopulation was
437 then divided using the intracellular PE straining into a 3A-FLAG* positive and negative populations

438 and percentages of positive and negative cells of the total single cells were reported. Experiments
439 were performed in duplicate.

440 **Immunofluorescence microscopy**

441 HeLa cells were plated in 12 well plates containing 12 mm no.1.5 circular glass coverslips
442 (Fisherbrand) at a cell density of 60,000 per well and transfected with FLAG*-3A or an empty
443 plasmid control. Cells were fixed 24 h post-transfection with 2% (w/v) paraformaldehyde (Sigma)
444 for 30 min, permeabilized with 0.1% (w/v) Triton X-100, and blocked with 2% (w/v) BSA, 0.1%
445 (w/v) Triton X-100 in PBS (blocking buffer). After blocking, cells were incubated with rabbit α-
446 GBF1 (abcam; ab86071 1:1000 dilution) and mouse α-FLAG (Sigma F1804; 1:200 dilution) for 1
447 h followed by 1 h staining with secondary antibodies goat α-rabbit AlexaFluor-488, and goat α-
448 mouse AlexaFluor-594 (Invitrogen), used at a 1/1000 dilution. The coverslips were mounted on
449 Superfrost™ microscope slides (Fisherbrand), nuclei were stained with DAPI, and the cells were
450 cleared with Prolong Glass (Invitrogen). Images were acquired with a 100× NA 1.4 objective
451 (Olympus) on a DeltaVision Elite High-Resolution Microscope (GE Healthcare Life Sciences).
452 Fluorescence excitation was driven by an Insight SSI solid state light engine (Cytiva) and
453 fluorescence emission was collected by a CoolSnap HQ2 CCD camera (Photometrics). The sides
454 of each CCD pixel are 6.45 μm. Image z stacks were acquired with 0.2 μm steps and 25 - 27
455 images per stack. Images were deconvolved with a classic maximum likelihood estimation
456 algorithm using Huygens software (Scientific Volume Imaging; The Netherlands) and
457 experimentally determined point spread functions captured by imaging PS-Speck™ beads
458 (Invitrogen) under experimental conditions, as done previously (Mast et al., 2018; Vijayan et al.,
459 2019).

460 **Image quantification**

461 Images were processed using Imaris software (Bitplane) to quantify the number of GBF1 puncta
462 per cell. Initial cell segmentation was performed by summing the fluorescent intensities from all

463 channels and using the 'Surface' command to threshold the images. This segmentation was
464 refined using the 'Cell' command. Cell nuclei were defined using the DAPI channel and cell
465 boundaries defined using a watershed algorithm seed by the 'one nucleus per cell' function in
466 order to split touching cells. Next, the GBF1-488 channel was selected for detecting GBF1 puncta
467 using the 'detect vesicle' function. Statistical values for 'Vesicle intensity sum' and 'vesicle
468 distance to closest nucleus' for each GBF1 puncta per cell were exported for 42 cells from control
469 samples, and from 13 cells of 3A-FLAG* transfected cells. Distances of GBF1 puncta from the
470 nearest nucleus in 3A-FLAG* cells were compared to distances from control cells using Wilcoxon
471 rank-sum tests. Comparisons were made using all observed puncta and, separately, using only
472 puncta more than 20 mm from the closest nucleus.

473 **Coimmunoprecipitation**

474 HeLa cells were transfected with 1 µg DNA of each of the FLAG*-3A and an empty control
475 plasmid. At 24 h post-transfection, cells were lysed using mild sonication in IP lysis buffer (20 mM
476 HEPES, 1% (w/v) Triton X-100, 2 mM Magnesium chloride, 25 mM Sodium chloride, 110 mM
477 Potassium acetate, and 0.2% (v/v) antifoam B), and clarified by centrifugation at 100,000 *g* for 3
478 min. Total protein concentrations were measured using BCA assay and 100 µg of lysate from
479 each sample was used in the immunoprecipitation. 8 µg of α-FLAG (F3165, Sigma Aldrich) was
480 conjugated to 10 mg epoxy-coated M-270 magnetic beads (ThermoFisher Scientific) (Cristea and
481 Chait, 2011). The α-FLAG conjugated beads were washed and re-suspended in IP lysis buffer,
482 and 3 mg bead aliquots were added to the clarified lysates. Lysates were incubated with magnetic
483 beads overnight at 4 ˚C. After three washes with IP lysis buffer, bound proteins were eluted with
484 50 µl 1× LDS sample buffer and resolved on 4-20% Bis-Tris NuPAGE gel. Additionally, ~10% of
485 the eluate volume was resolved on a 3-8% Tris-Tricine gel to confirm expression and enrichment
486 of the immunoprecipitated 3A-FLAG* bait. Proteins were transferred to PVDF membranes and

487 immunoblotted with α-GBF1 (ab86071; abcam, at 1:1000 dilution) and HRP conjugated α-FLAG
488 (A8592; Millipore Sigma 1:2000 dilution). The experiment was performed in triplicate.

489 **Cell viability assay**

490 Cell viability assays were performed in 96-well plates using the CellTiterBlue reagent (Promega).
491 Working concentrations of GCA were prepared by diluting a 10 mM DMSO-solubilized stock in
492 complete media. Equimolar solutions lacking the drug were prepared by diluting neat DMSO.
493 Cells were incubated in 100 µl of GCA or DMSO working solutions for 48 h before 20 µl of the
494 CellTiterBlue reagent was added, and fluorescence was measured 4 h-post addition using a
495 Synergy HTX Multi-mode plate reader (BioTek). The metabolically active cells convert the blue
496 redox reagent into its fluorescent product with the number of live cells directly proportional to the
497 intensity of the fluorescent product. Fluorescence measurements from the drug-treated samples
498 are normalized using the signal from matched DMSO-treated samples.

499 For the viability assay validating *GBF1*-SL candidates, 20,000 cells of each gene KD cell
500 line (*ARF1* KD, *HSP90AB* KD, *CSK* KD, *PRKAA1* KD, *ARF4* KD, *MSMO1* KD) were seeded per
501 well in 200 µl media. The next day, the media was replaced with 100 µl of GCA or DMSO at 1.5
502 µg/ml and 4 µg/ml, incubated for 48 h, and cell viability was measured as described above.
503 Normalized cell viabilities of the KD cells were compared to that of the *MSMO1* KD controls.

504 For generating GCA dose response curves we used an automated high throughput liquid
505 handling system (PipetteMax, Gilson) for co-plating cells and the drug. Stock solutions of GCA or
506 DMSO were prepared in complete media at a concentration of 200 µM, and serially diluted in cell-
507 containing media of *ARF1* KD and *MSMO1* KD (400,000 cells/ml) to obtain 0–100 µM of
508 GCA/DMSO with 20,000 cells/ well, plated in triplicate. Cell viabilities were measured 48 h post-
509 incubation as described above. GCA dose response curves were plotted with GraphPad Prism 8.

510 For the proof-of-concept SL viability experiments, 60,000 cells of *ARF1* KD and *MSMO1*
511 KD were seeded in a 6-well plate and transfected the following day with 3A-FLAG* or an empty

512 plasmid control. After 24 h post transfection, cells were harvested, counted, and plated in 96-well
513 plate at a density of 5000 cells per well. The remaining cells were processed for flow cytometry
514 analysis to measure transfection efficiencies. Cell viabilities were measured 48 h post-transfection
515 using CellTiterBlue reagent, as described above. Absolute cell viabilities of *ARF1* KD and *MSMO1*
516 KD cells were compared using a multiple T-test, i.e., the two-stage step-up method of Benjamini,
517 Krieser and Yekutieli (Benjamini et al., 2006), in GraphPad Prism 8. The experiment was
518 performed in triplicate.

519 **Online supplemental material**

520 Table S1 contains supporting data reporting the GCA CRISPR screen results for the 19,029
521 Refseq genes. For each gene, we report the RANKS (Robust Analytics and Normalization for
522 Knockout Screens) score, associated p-values, the FDR, the number sgRNA considered for the
523 analysis, and the gene-level $\log_2$ fold changes. Fig. S1 contains the results from a GCA dose-
524 response assay used to determine the concentration of GCA in the CRISPR screen reported in
525 Fig 2. Fig. S2 contains supporting immunoblots that show the efficiency of the shRNA-mediated
526 protein depletion for the *ARF1*, *MSMO1*, *ARF4*, *PRKAA1*, *CSK*, and *HSP90* KD cell lines.

527 **Acknowledgments**

528 This work was supported by National Institutes of Health grants R01 GM112108 and P41
529 GM109824 to J.D. Aitchison, and R21 AI151344 to A. Kaushansky and foundation grant FDN-
530 167277 from the Canadian Institutes of Health Research to M. Tyers/

531 J.D. Aitchison, A.T. Navare, F.D. Mast, M. Tyers, T. Bertomeu, P. Olivier, and M. Neal are
532 inventors on a provisional patent disclosing synthetic lethal approaches described in this
533 manuscript.

534 Author Contributions: J.D. Aitchison, F.D. Mast, and A.T. Navare wrote the original draft of the
535 manuscript. F.D Mast, A.T. Navare, J.P. Olivier, L.N. Carpp, T. Bertomeu, and J. Coulombe-

Huntington designed and performed the experiments and interpreted results. M. Neal analyzed data and interpreted results. J.D. Aitchison, A. Kaushansky, and M. Tyers designed and oversaw experiments and revised manuscript drafts. All authors read and commented on the manuscript.

539 **REFERENCES**

540 Basler, C.F., N.J. Krogan, D.W. Leung, and G.K. Amarasinghe. 2019. Virus and host interactions
541 critical for filoviral RNA synthesis as therapeutic targets. *Antiviral Res.* 162:90–100.
542 doi:10.1016/j.antiviral.2018.12.006.

543 Beijersbergen, R.L., L.F.A. Wessels, and R. Bernards. 2017. Synthetic lethality in cancer
544 therapeutics. *Annu. Rev. Cancer Biol.* doi:10.1146/annurev-cancerbio-042016-073434.

545 Beller, M., C. Sztalryd, N. Southall, M. Bell, H. Jäckle, D.S. Auld, and B. Oliver. 2008. COPI
546 complex is a regulator of lipid homeostasis. *PLoS Biol.* 6:2530–2549.
547 doi:10.1371/journal.pbio.0060292.

548 Belov, G.A., N. Altan-Bonnet, G. Kovtunovych, C.L. Jackson, J. Lippincott-Schwartz, and E.
549 Ehrenfeld. 2007. Hijacking Components of the Cellular Secretory Pathway for Replication of
550 Poliovirus RNA. *J. Virol.* 81:558–567. doi:10.1128/jvi.01820-06.

551 Belov, G.A., Q. Feng, K. Nikovics, C.L. Jackson, and E. Ehrenfeld. 2008a. A critical role of a
552 cellular membrane traffic protein in poliovirus RNA replication. *PLoS Pathog.*
553 doi:10.1371/journal.ppat.1000216.

554 Belov, G.A., Q. Feng, K. Nikovics, C.L. Jackson, and E. Ehrenfeld. 2008b. A critical role of a
555 cellular membrane traffic protein in poliovirus RNA replication. *PLoS Pathog.* 4.
556 doi:10.1371/journal.ppat.1000216.

557 Belov, G.A., M.H. Fogg, and E. Ehrenfeld. 2005. Poliovirus Proteins Induce Membrane
558 Association of GTPase ADP-Ribosylation Factor. *J. Virol.* 79:7207–7216.
559 doi:10.1128/jvi.79.11.7207-7216.2005.

560 Benjamini, Y., A.M. Krieger, and D. Yekutieli. 2006. Adaptive linear step-up procedures that
561 control the false discovery rate. *Biometrika*. doi:10.1093/biomet/93.3.491.

562 Bertomeu, T., J. Coulombe-Huntington, A. Chatr-aryamontri, K.G. Bourdages, E. Coyaud, B.
563 Raught, Y. Xia, and M. Tyers. 2018. A High-Resolution Genome-Wide CRISPR/Cas9
564 Viability Screen Reveals Structural Features and Contextual Diversity of the Human Cell-
565 Essential Proteome. *Mol. Cell. Biol.* 38. doi:10.1128/mcb.00302-17.

566 Boone, C., H. Bussey, and B.J. Andrews. 2007. Exploring genetic interactions and networks with
567 yeast. *Nat. Rev. Genet.* doi:10.1038/nrg2085.

568 Brass, A.L., D.M. Dykxhoorn, Y. Benita, N. Yan, A. Engelman, R.J. Xavier, J. Lieberman, and S.J.
569 Elledge. 2008. Identification of host proteins required for HIV infection through a functional
570 genomic screen. *Science (80-.).* 319:921–926. doi:10.1126/science.1152725.

571 Brown, M.B., and A.B. Forsythe. 1974. Robust tests for the equality of variances. *J. Am. Stat.*
572 *Assoc.* doi:10.1080/01621459.1974.10482955.

573 Bryant, H.E., N. Schultz, H.D. Thomas, K.M. Parker, D. Flower, E. Lopez, S. Kyle, M. Meuth, N.J.
574 Curtin, and T. Helleday. 2005. Specific killing of BRCA2-deficient tumours with inhibitors of
575 poly(ADP-ribose) polymerase. *Nature*. doi:10.1038/nature03443.

576 Carpp, L.N., R.S. Rogers, R.L. Moritz, and J.D. Aitchison. 2014. Quantitative proteomic analysis
577 of host-virus interactions reveals a role for golgi brefeldin a resistance factor 1 (GBF1) in
578 dengue infection. *Mol. Cell. Proteomics*. 13:2836–2854. doi:10.1074/mcp.M114.038984.

579 Carrasco-Hernandez, R., R. Jácome, Y.L. Vidal, and S.P. de León. 2017. Are RNA viruses
580 candidate agents for the next global pandemic? A review. *ILAR J.* 58:343–358.
581 doi:10.1093/ilar/ilx026.

582 Chantalat, S., R. Courbeyrette, F. Senic-Matuglia, C.L. Jackson, B. Goud, and A. Peyroche. 2003.

583 A novel Golgi membrane protein is a partner of the ARF exchange factors Gea1p and Gea2p.
584 *Mol. Biol. Cell*. doi:10.1091/mbc.E02-10-0693.

585 de Chassey, B., L. Meyniel-Schicklin, J. Vonderscher, P. André, and V. Lotteau. 2014. Virus-host
586 interactomics: New insights and opportunities for antiviral drug discovery. *Genome Med.* 6.
587 doi:10.1186/s13073-014-0115-1.

588 Citterio, C., A. Vichi, G. Pacheco-Rodriguez, A.M. Aponte, J. Moss, and M. Vaughan. 2008.
589 Unfolded protein response and cell death after depletion of brefeldin A-inhibited guanine
590 nucleotide-exchange protein GBF. *Proc. Natl. Acad. Sci. U. S. A.* 105:2877–2882.
591 doi:10.1073/pnas.0712224105.

592 Claude, A., B.-P. Zhao, C.E. Kuziemsky, S. Dahan, S.J. Berger, J.-P. Yan, A.D. Armold, E.M.
593 Sullivan, and P. Melançon. 1999. GBF1: A Novel Golgi-associated BFA-resistant Guanine
594 Nucleotide Exchange Factor That Displays Specificity for ADP-ribosylation Factor 5. 146.
595 71–84 pp.

596 Cotto, K.C., A.H. Wagner, Y.Y. Feng, S. Kiwala, A.C. Coffman, G. Spies, A. Wollam, N.C. Spies,
597 O.L. Griffith, and M. Griffith. 2018. DGIdb 3.0: A redesign and expansion of the drug-gene
598 interaction database. *Nucleic Acids Res.* doi:10.1093/nar/gkx1143.

599 Cristea, I.M., and B.T. Chait. 2011. Conjugation of magnetic beads for immunopurification of
600 protein complexes. *Cold Spring Harb. Protoc.* doi:10.1101/pdb.prot5610.

601 Dixon, S.J., B.J. Andrews, and C. Boone. 2009. Exploring the conservation of synthetic lethal
602 genetic interaction networks. *Commun. Integr. Biol.* doi:10.4161/cib.7501.

603 Dobzhansky, T. 1946. Genetics of natural populations; recombination and variability in
604 populations of Drosophila pseudoobscura. *Genetics*.

605 Donaldson, J.G., and C.L. Jackson. 2011. ARF family G proteins and their regulators: Roles in
606 membrane transport, development and disease. *Nat. Rev. Mol. Cell Biol.* 12:362–375.
607 doi:10.1038/nrm3117.

608 Drees, B.L., V. Thorsson, G.W. Carter, A.W. Rives, M.Z. Raymond, I. Avila-Campillo, P. Shannon,
609 and T. Galitski. 2005. Derivation of genetic interaction networks from quantitative phenotype
610 data. *Genome Biol.* doi:10.1186/gb-2005-6-4-r38.

611 Ellong, E.N., K.G. Soni, Q.-T. Bui, R. Sougrat, M.-P. Golinelli-Cohen, and C.L. Jackson. 2011.
612 Interaction between the Triglyceride Lipase ATGL and the Arf1 Activator GBF1. *PLoS One*.
613 6:e21889. doi:10.1371/journal.pone.0021889.

614 Enard, D., and D.A. Petrov. 2020. Ancient RNA virus epidemics through the lens of recent
615 adaptation in human genomes. *Philos. Trans. R. Soc. Lond. B. Biol. Sci.*
616 doi:10.1098/rstb.2019.0575.

617 Farhat, R., M. Ankavay, N. Lebsir, J. Gouttenoire, C.L. Jackson, C. Wychowski, D. Moradpour, J.
618 Dubuisson, Y. Rouillé, and L. Cocquerel. 2018. Identification of GBF1 as a cellular factor
619 required for hepatitis E virus RNA replication. *Cell. Microbiol.* 20. doi:10.1111/cmi.12804.

620 Farmer, H., H. McCabe, C.J. Lord, A.H.J. Tutt, D.A. Johnson, T.B. Richardson, M. Santarosa,
621 K.J. Dillon, I. Hickson, C. Knights, N.M.B. Martin, S.P. Jackson, G.C.M. Smith, and A.
622 Ashworth. 2005. Targeting the DNA repair defect in BRCA mutant cells as a therapeutic
623 strategy. *Nature*. 434:917–921. doi:10.1038/nature03445.

624 García-Mata, R., and E. Sztul. 2003. The membrane-tethering protein p115 interacts with GBF1,
625 an ARF guanine-nucleotide-exchange factor. *EMBO Rep.* 4:320–325.
626 doi:10.1038/sj.embor.embor762.

627 Gaur, P., A. Munjal, and S.K. Lal. 2011. Influenza virus and cell signaling pathways. *Med. Sci.*
628 *Monit.* 17. doi:10.12659/MSM.881801.

629 Gordon, D.E., J. Hiatt, M. Bouhaddou, V. V. Rezelj, S. Ulferts, H. Braberg, A.S. Jureka, K.
630 Obernier, J.Z. Guo, J. Batra, R.M. Kaake, A.R. Weckstein, T.W. Owens, M. Gupta, S.
631 Pourmal, E.W. Titus, M. Cakir, M. Soucheray, M. McGregor, Z. Cakir, G. Jang, M.J. O'Meara,
632 T.A. Tummino, Z. Zhang, H. Foussard, A. Rojc, Y. Zhou, D. Kuchenov, R. Hüttenhain, J. Xu,
633 M. Eckhardt, D.L. Swaney, J.M. Fabius, M. Ummadi, B. Tutuncuoglu, U. Rathore, M. Modak,
634 P. Haas, K.M. Haas, Z.Z.C. Naing, E.H. Pulido, Y. Shi, I. Barrio-Hernandez, D. Memon, E.
635 Petsalaki, A. Dunham, M.C. Marrero, D. Burke, C. Koh, T. Vallet, J.A. Silvas, C.M. Azumaya,
636 C. Billesbølle, A.F. Brilot, M.G. Campbell, A. Diallo, M.S. Dickinson, D. Diwanji, N. Herrera,
637 N. Hoppe, H.T. Kratochvil, Y. Liu, G.E. Merz, M. Moritz, H.C. Nguyen, C. Nowotny, C.
638 Puchades, A.N. Rizo, U. Schulze-Gahmen, A.M. Smith, M. Sun, I.D. Young, J. Zhao, D.
639 Asarnow, J. Biel, A. Bowen, J.R. Braxton, J. Chen, C.M. Chio, U.S. Chio, I. Deshpande, L.
640 Doan, B. Faust, S. Flores, M. Jin, K. Kim, V.L. Lam, F. Li, J. Li, Y.-L. Li, Y. Li, X. Liu, M. Lo,
641 K.E. Lopez, A.A. Melo, F.R. Moss, P. Nguyen, J. Paulino, et al. 2020a. Comparative host-
642 coronavirus protein interaction networks reveal pan-viral disease mechanisms. *Science (80-*
643 *.).* doi:10.1126/science.abe9403.

644 Gordon, D.E., G.M. Jang, M. Bouhaddou, J. Xu, K. Obernier, K.M. White, M.J. O'Meara, V. V.
645 Rezelj, J.Z. Guo, D.L. Swaney, T.A. Tummino, R. Hüttenhain, R.M. Kaake, A.L. Richards, B.
646 Tutuncuoglu, H. Foussard, J. Batra, K. Haas, M. Modak, M. Kim, P. Haas, B.J. Polacco, H.
647 Braberg, J.M. Fabius, M. Eckhardt, M. Soucheray, M.J. Bennett, M. Cakir, M.J. McGregor,
648 Q. Li, B. Meyer, F. Roesch, T. Vallet, A. Mac Kain, L. Miorin, E. Moreno, Z.Z.C. Naing, Y.
649 Zhou, S. Peng, Y. Shi, Z. Zhang, W. Shen, I.T. Kirby, J.E. Melnyk, J.S. Chorba, K. Lou, S.A.
650 Dai, I. Barrio-Hernandez, D. Memon, C. Hernandez-Armenta, J. Lyu, C.J.P. Mathy, T. Perica,
651 K.B. Pilla, S.J. Ganesan, D.J. Saltzberg, R. Rakesh, X. Liu, S.B. Rosenthal, L. Calviello, S.
652 Venkataramanan, J. Liboy-Lugo, Y. Lin, X.P. Huang, Y.F. Liu, S.A. Wankowicz, M. Bohn, M.
653 Safari, F.S. Ugur, C. Koh, N.S. Savar, Q.D. Tran, D. Shengjuler, S.J. Fletcher, M.C. O'Neal,
654 Y. Cai, J.C.J. Chang, D.J. Broadhurst, S. Klippsten, P.P. Sharp, N.A. Wenzell, D. Kuzuoglu-
655 Ozturk, H.Y. Wang, R. Trenker, J.M. Young, D.A. Cavero, J. Hiatt, T.L. Roth, U. Rathore, A.
656 Subramanian, J. Noack, M. Hubert, R.M. Stroud, A.D. Frankel, O.S. Rosenberg, K.A. Verba,
657 D.A. Agard, M. Ott, et al. 2020b. A SARS-CoV-2 protein interaction map reveals targets for
658 drug repurposing. *Nature*. 583:459–468. doi:10.1038/s41586-020-2286-9.

659 Goueslain, L., K. Alsaleh, P. Horellou, P. Roingeard, V. Descamps, G. Duverlie, Y. Ciczora, C.
660 Wychowski, J. Dubuisson, and Y. Rouille. 2010. Identification of GBF1 as a Cellular Factor
661 Required for Hepatitis C Virus RNA Replication. *J. Virol.* 84:773–787. doi:10.1128/jvi.01190-
662 09.

663 Guo, Y., T.C. Walther, M. Rao, N. Stuurman, G. Goshima, K. Terayama, J.S. Wong, R.D. Vale,
664 P. Walter, and R. V. Farese. 2008. Functional genomic screen reveals genes involved in
665 lipid-droplet formation and utilization. *Nature*. 453:657–661. doi:10.1038/nature06928.

666 Hartman IV, J.L., B. Garvik, and L. Hartwell. 2001. Principles for the Buffering of Genetic Variation.
667 *Princ. Buffering Genet. Var.* doi:10.1126/science.1056072.

668 Hartwell, L.H., P. Szankasi, C.J. Roberts, A.W. Murray, and S.H. Friend. 1997. Integrating genetic
669 approaches into the discovery of anticancer drugs. *Science (80-.).* 278:1064–1068.
670 doi:10.1126/science.278.5340.1064.

671 Heaton, S.M. 2019. Harnessing host–virus evolution in antiviral therapy and immunotherapy. *Clin.*
672 *Transl. Immunol.* 8. doi:10.1002/cti2.1067.

673 Horlbeck, M.A., A. Xu, M. Wang, N.K. Bennett, C.Y. Park, D. Bogdanoff, B. Adamson, E.D. Chow,

674 M. Kampmann, T.R. Peterson, K. Nakamura, M.A. Fischbach, J.S. Weissman, and L.A.
675 Gilbert. 2018. Mapping the Genetic Landscape of Human Cells. *Cell*.
676 doi:10.1016/j.cell.2018.06.010.

677 Irwin, K.K., N. Renzette, T.F. Kowalik, and J.D. Jensen. 2016. Antiviral drug resistance as an
678 adaptive process. *Virus Evol.* 2:vew014. doi:10.1093/ve/vew014.

679 Kaczmarek, B., J.M. Verbavatz, and C.L. Jackson. 2017. GBF1 and Arf1 function in vesicular
680 trafficking, lipid homoeostasis and organelle dynamics. *Biol. Cell*.
681 doi:10.1111/boc.201700042.

682 Kaelin, W.G. 2005. The concept of synthetic lethality in the context of anticancer therapy. *Nat.*
683 *Rev. Cancer*. doi:10.1038/nrc1691.

684 Kaufmann, S.H.E., A. Dorhoi, R.S. Hotchkiss, and R. Bartenschlager. 2018. Host-directed
685 therapies for bacterial and viral infections. *Nat. Rev. Drug Discov.* 17:35–56.
686 doi:10.1038/nrd.2017.162.

687 Kawamoto, K., Y. Yoshida, H. Tamaki, S. Torii, C. Shinotsuka, S. Yamashina, and K. Nakayama.
688 2002. GBF1, a Guanine Nucleotide Exchange Factor for ADP-Ribosylation Factors, is
689 Localized to the cis-Golgi and Involved in Membrane Association of the COPI Coat. *Traffic*.
690 3:483–495.

691 Krishnan, M.N., and M.A. Garcia-Blanco. 2014. Targeting host factors to treat West Nile and
692 dengue viral infections. *Viruses*. 6:683–708. doi:10.3390/v6020683.

693 Lanke, K.H.W., H.M. van der Schaar, G.A. Belov, Q. Feng, D. Duijsings, C.L. Jackson, E.
694 Ehrenfeld, and F.J.M. van Kuppeveld. 2009. GBF1, a Guanine Nucleotide Exchange Factor
695 for Arf, Is Crucial for Coxsackievirus B3 RNA Replication. *J. Virol.* 83:11940–11949.
696 doi:10.1128/jvi.01244-09.

697 Laurent, E.M., Y. Sofianatos, A. Komarova, J.-P. Gimeno, P. Samavarchi Tehrani, D.-K. Kim, H.
698 Abdouni, M. Duhamel, P. Cassonnet, J.J. Knapp, D. Kuang, A. Chawla, D. Sheykhkarimli,
699 A. Rayhan, R. Li, O. Pogoutse, D.E. Hill, M.A. Calderwood, P. Falter-Braun, P. Aloy, U. Stelzl,
700 M. Vidal, A.-C. Gingras, G.A. Pavlopoulos, S. Van Der Werf, I. Fournier, F.P. Roth, M. Salzet,
701 C. Demeret, Y. Jacob, and E. Coyaud. 2020. Global BioID-based SARS-CoV-2 proteins
702 proximal interactome unveils novel ties between viral polypeptides and host factors involved
703 in multiple COVID19-associated mechanisms. *bioRxiv*.

704 Liang, J.O., and S. Kornfeld. 1997. Comparative activity of ADP-ribosylation factor family
705 members in the early steps of coated vesicle formation on rat liver Golgi membranes. *J. Biol.*
706 *Chem.* 272:4141–4148. doi:10.1074/jbc.272.7.4141.

707 Litton, J.K., H.S. Rugo, J. Ettl, S.A. Hurvitz, A. Gonçalves, K.H. Lee, L. Fehrenbacher, R.
708 Yerushalmi, L.A. Mina, M. Martin, H. Roché, Y.H. Im, R.G.W. Quek, D. Markova, I.C. Tudor,
709 A.L. Hannah, W. Eiermann, and J.L. Blum. 2018. Talazoparib in patients with advanced
710 breast cancer and a germline BRCA mutation. *N. Engl. J. Med.*
711 doi:10.1056/NEJMoa1802905.

712 Lum, K.K., and I.M. Cristea. 2016. Proteomic approaches to uncovering virus-host protein
713 interactions during the progression of viral infection. *Expert Rev. Proteomics*. 13:325–340.
714 doi:10.1586/14789450.2016.1147353.

715 Manolea, F., A. Claude, J. Chun, J. Rosas, and P. Melançon. 2008. Distinct functions for Arf
716 guanine nucleotide exchange factors at the Golgi complex: GBF1 and BIGs are required for
717 assembly and maintenance of the Golgi stack and trans-Golgi network, respectively. *Mol.*
718 *Biol. Cell*. 19:523–535. doi:10.1091/mbc.E07-04-0394.

719 Martínez, J., F. Arnoldi, E. Schraner, C. Eichwald, D. Silva-Ayala, E. Lee, E. Sztul, Ó. Burrone, S.
720 López, and C. Arias. 2019. The guanine nucleotide exchange factor GBF1 participates in
721 rotavirus replication. *bioRxiv*. 619924. doi:10.1101/619924.

722 Mast, F.D., T. Herricks, K.M. Strehler, L.R. Miller, R.A. Saleem, R.A. Rachubinski, and J.D.
723 Aitchison. 2018. ESC RT-III is required for scissioning new peroxisomes from the
724 endoplasmic reticulum. *J. Cell Biol.* 217:2087–2102. doi:10.1083/jcb.201706044.

725 Mast, F.D., A.T. Navare, A.M. van der Sloot, J. Coulombe-Huntington, M.P. Rout, N.S. Baliga, A.
726 Kaushansky, B.T. Chait, A. Aderem, C.M. Rice, A. Sali, M. Tyers, and J.D. Aitchison. 2020.
727 Crippling life support for SARS-CoV-2 and other viruses through synthetic lethality. *J. Cell*
728 *Biol.* 219. doi:10.1083/jcb.202006159.

729 McManus, K.J., I.J. Barrett, Y. Nouhi, and P. Hieter. 2009. Specific synthetic lethal killing of
730 RAD54B-deficient human colorectal cancer cells by FEN1 silencing. *Proc. Natl. Acad. Sci.*
731 *U. S. A.* doi:10.1073/pnas.0813414106.

732 Mendes-Pereira, A.M., S.A. Martin, R. Brough, A. McCarthy, J.R. Taylor, J.S. Kim, T. Waldman,
733 C.J. Lord, and A. Ashworth. 2009. Synthetic lethal targeting of PTEN mutant cells with PARP
734 inhibitors. *EMBO Mol. Med.* doi:10.1002/emmm.200900041.

735 Meyniel-Schicklin, L., B. De Chassey, P. André, and V. Lotteau. 2012. Viruses and interactomes
736 in translation. *Mol. Cell. Proteomics*. doi:10.1074/mcp.M111.014738.

737 Nakai, W., Y. Kondo, A. Saitoh, T. Naito, K. Nakayama, and H.W. Shin. 2013. ARF1 and ARF4
738 regulate recycling endosomal morphology and retrograde transport from endosomes to the
739 Golgi apparatus. *Mol. Biol. Cell*. doi:10.1091/mbc.E13-04-0197.

740 Navratil, V., B. De chassey, L. Meyniel, S. Delmotte, C. Gautier, P. André, V. Lotteau, and C.
741 Rabourdin-Combe. 2009. VirHostNet: A knowledge base for the management and the
742 analysis of proteome-wide virus-host interaction networks. *Nucleic Acids Res.*
743 doi:10.1093/nar/gkn794.

744 Nijman, S.M.B. 2011a. Synthetic lethality: General principles, utility and detection using genetic
745 screens in human cells. *FEBS Lett.* 585:1–6. doi:10.1016/j.febslet.2010.11.024.

746 Nijman, S.M.B. 2011b. Synthetic lethality: General principles, utility and detection using genetic
747 screens in human cells. *FEBS Lett.* 585:1–6. doi:10.1016/j.febslet.2010.11.024.

748 Okada, M. 2012. Regulation of the Src family kinases by Csk. *Int. J. Biol. Sci.* 8:1385–1397.
749 doi:10.7150/ijbs.5141.

750 Pennings, P.S. 2013. HIV drug resistance: Problems and perspectives. *Infect. Dis. Rep.* 5:21–25.
751 doi:10.4081/idr.2013.s1.e5.

752 Pfefferle, S., J. Schöpf, M. Kögl, C.C. Friedel, M.A. Müller, J. Carbajo-Lozoya, T. Stellberger, E.
753 von Dall'Armi, P. Herzog, S. Kallies, D. Niemeyer, V. Ditt, T. Kuri, R. Züst, K. Pumpor, R.
754 Hilgenfeld, F. Schwarz, R. Zimmer, I. Steffen, F. Weber, V. Thiel, G. Herrler, H.-J. Thiel, C.
755 Schwegmann-Weßels, S. Pöhlmann, J. Haas, C. Drosten, and A. von Brunn. 2011. The
756 SARS-Coronavirus-Host Interactome: Identification of Cyclophilins as Target for Pan-
757 Coronavirus Inhibitors. *PLoS Pathog.* 7:e1002331. doi:10.1371/journal.ppat.1002331.

758 Prussia, A., P. Thepchatri, J.P. Snyder, and R.K. Plemper. 2011. Systematic approaches towards
759 the development of host-directed antiviral therapeutics. *Int. J. Mol. Sci.*
760 doi:10.3390/ijms12064027.

761 Reiling, J.H., A.J. Olive, S. Sanyal, J.E. Carette, T.R. Brummelkamp, H.L. Ploegh, M.N.
762 Starnbach, and D.M. Sabatini. 2013. A Creb3–arf4 Signalling Pathway Mediates the

763 Response to Golgi Stress and Susceptibility to Pathogens. *Nat. Cell Biol.*
764 doi:10.1038/ncb2865.

765 Richards, A.L., J.A.P. Soares-Martins, G.T. Riddell, and W.T. Jackson. 2014. Generation of
766 unique poliovirus RNA replication organelles. *MBio*. 5. doi:10.1128/mBio.00833-13.

767 Rosenberg, R. 2015. Detecting the emergence of novel, zoonotic viruses pathogenic to humans.
768 72:1115–1125. doi:10.1007/s00018-014-1785-y.

769 Rowlands, M., C. McAndrew, C. Prodromou, L. Pearl, A. Kalusa, K. Jones, P. Workman, and W.
770 Aherne. 2010. Detection of the ATPase activity of the molecular chaperones Hsp90 and
771 Hsp72 using the transcreener™ ADP assay kit. *J. Biomol. Screen.* 15:279–286.
772 doi:10.1177/1087057109360253.

773 Saeed, M., S. Kapell, N.T. Hertz, X. Wu, K. Bell, A.W. Ashbrook, M.T. Mark, H.A. Zebroski, M.L.
774 Neal, M. Flodström-Tullberg, M.R. MacDonald, J.D. Aitchison, H. Molina, and C.M. Rice.
775 2020. Defining the proteolytic landscape during enterovirus infection. *PLOS Pathog.*
776 16:e1008927. doi:10.1371/journal.ppat.1008927.

777 Sáenz, J.B., W.J. Sun, J.W. Chang, J. Li, B. Bursulaya, N.S. Gray, and D.B. Haslam. 2009.
778 Golgicide A reveals essential roles for GBF1 in Golgi assembly and function. *Nat. Chem.*
779 *Biol.* 5:157–165. doi:10.1038/nchembio.144.

780 Sanjuán, R., M.R. Nebot, N. Chirico, L.M. Mansky, and R. Belshaw. 2010. Viral Mutation Rates.
781 *J. Virol.* 84:9733–9748. doi:10.1128/jvi.00694-10.

782 Sanli, T., G.R. Steinberg, G. Singh, and T. Tsakiridis. 2014. AMP-activated protein kinase (AMPK)
783 beyond metabolism: A novel genomic stress sensor participating in the DNA damage
784 response pathway. *Cancer Biol. Ther.* 15:156–169. doi:10.4161/cbt.26726.

785 Shannon, P., A. Markiel, O. Ozier, N.S. Baliga, J.T. Wang, D. Ramage, N. Amin, B. Schwikowski,
786 and T. Ideker. 2003. Cytoscape: A software Environment for integrated models of
787 biomolecular interaction networks. *Genome Res.* doi:10.1101/gr.1239303.

788 Soni, K.G., G.A. Mardones, R. Sougrat, E. Smirnova, C.L. Jackson, and J.S. Bonifacino. 2009.
789 Coatomer-dependent protein delivery to lipid droplets. *J. Cell Sci.* 122:1834–1841.
790 doi:10.1242/jcs.045849.

791 Stukalov, A., V. Girault, V. Grass, V. Bergant, O. Karayel, C. Urban, D.A. Haas, Y. Huang, L.
792 Oubraham, A. Wang, S.M. Hamad, A. Piras, M. Tanzer, F.M. Hansen, T. Enghleitner, M.
793 Reinecke, T.M. Lavacca, R. Ehmann, R. Wölfel, J. Jores, B. Kuster, U. Protzer, R. Rad, J.
794 Ziebuhr, V. Thiel, P. Scaturro, M. Mann, and A. Pichlmair. 2020. Multi-level proteomics
795 reveals host-perturbation strategies of SARS-CoV-2 and SARS-CoV. *bioRxiv*.
796 2020.06.17.156455. doi:10.1101/2020.06.17.156455.

797 Surma, M.A., C. Klose, D. Peng, M. Shales, C. Mrejen, A. Stefanko, H. Braberg, D.E. Gordon, D.
798 Vorkel, C.S. Ejsing, R. Farese, K. Simons, N.J. Krogan, and R. Ernst. 2013. A lipid E-MAP
799 identifies Ubx2 as a critical regulator of lipid saturation and lipid bilayer stress. *Mol. Cell*.
800 doi:10.1016/j.molcel.2013.06.014.

801 Szklarczyk, D., A.L. Gable, D. Lyon, A. Junge, S. Wyder, J. Huerta-Cepas, M. Simonovic, N.T.
802 Doncheva, J.H. Morris, P. Bork, L.J. Jensen, and C. Von Mering. 2019. STRING v11:
803 Protein-protein association networks with increased coverage, supporting functional
804 discovery in genome-wide experimental datasets. *Nucleic Acids Res.*
805 doi:10.1093/nar/gky1131.

806 Teterina, N.L., Y. Pinto, J.D. Weaver, K.S. Jensen, and E. Ehrenfeld. 2011. Analysis of Poliovirus
807 Protein 3A Interactions with Viral and Cellular Proteins in Infected Cells. *J. Virol.*

808 doi:10.1128/jvi.02398-10.

809 Thaker, S.K., J. Ch'ng, and H.R. Christofk. 2019. Viral hijacking of cellular metabolism. *BMC Biol.*
810 17:59. doi:10.1186/s12915-019-0678-9.

811 Turner, N.C., C.J. Lord, E. Iorns, R. Brough, S. Swift, R. Elliott, S. Rayter, A.N. Tutt, and A.
812 Ashworth. 2008. A synthetic lethal siRNA screen identifying genes mediating sensitivity to a
813 PARP inhibitor. *EMBO J.* doi:10.1038/emboj.2008.61.

814 Verheije, M.H., M. Raaben, M. Mari, E.G. Te Lintelo, F. Reggiori, F.J.M. Van Kuppeveld, P.J.M.
815 Rottier, and C.A.M. De Haan. 2008. Mouse hepatitis coronavirus RNA replication depends
816 on GBF1-mediated ARF1 activation. *PLoS Pathog.* 4. doi:10.1371/journal.ppat.1000088.

817 Vijayan, K., I. Cestari, F.D. Mast, E.K.K. Glennon, S.M. McDermott, H.S. Kain, A.M. Brokaw, J.D.
818 Aitchison, K. Stuart, and A. Kaushansky. 2019. Plasmodium Secretion Induces Hepatocyte
819 Lysosome Exocytosis and Promotes Parasite Entry. *iScience*. 21:603–611.
820 doi:10.1016/j.isci.2019.10.054.

821 van der Vries, E., M. Schutten, P. Fraaij, C. Boucher, and A. Osterhaus. 2013. Influenza virus
822 resistance to antiviral therapy. *In* Advances in Pharmacology. Academic Press Inc. 217–246.

823 Wang, T., J.J. Wei, D.M. Sabatini, and E.S. Lander. 2014. Genetic screens in human cells using
824 the CRISPR-Cas9 system. *Science (80-.).* doi:10.1126/science.1246981.

825 Welch, B.L. 1951. On the Comparison of Several Mean Values: An Alternative Approach.
826 *Biometrika*. doi:10.2307/2332579.

827 Wessels, E., D. Duijsings, K.H.W. Lanke, S.H.J. van Dooren, C.L. Jackson, W.J.G. Melchers, and
828 F.J.M. van Kuppeveld. 2006a. Effects of Picornavirus 3A Proteins on Protein Transport and
829 GBF1-Dependent COP-I Recruitment. *J. Virol.* 80:11852–11860. doi:10.1128/jvi.01225-06.

830 Wessels, E., D. Duijsings, K.H.W. Lanke, S.H.J. van Dooren, C.L. Jackson, W.J.G. Melchers, and
831 F.J.M. van Kuppeveld. 2006b. Effects of Picornavirus 3A Proteins on Protein Transport and
832 GBF1-Dependent COP-I Recruitment. *J. Virol.* 80:11852–11860. doi:10.1128/jvi.01225-06.

833 Wessels, E., D. Duijsings, K.H.W. Lanke, W.J.G. Melchers, C.L. Jackson, and F.J.M. van
834 Kuppeveld. 2007. Molecular Determinants of the Interaction between Coxsackievirus Protein
835 3A and Guanine Nucleotide Exchange Factor GBF1. *J. Virol.* 81:5238–5245.
836 doi:10.1128/jvi.02680-06.

837 Wessels, E., D. Duijsings, T.K. Niu, S. Neumann, V.M. Oorschot, F. de Lange, K.H.W. Lanke, J.
838 Klumperman, A. Henke, C.L. Jackson, W.J.G. Melchers, and F.J.M. van Kuppeveld. 2006c.
839 A Viral Protein that Blocks Arf1-Mediated COP-I Assembly by Inhibiting the Guanine
840 Nucleotide Exchange Factor GBF1. *Dev. Cell*. 11:191–201.
841 doi:10.1016/j.devcel.2006.06.005.

842 Wiltshire, T.D., C.A. Lovejoy, T. Wang, F. Xia, M.J. O'Connor, and D. Cortez. 2010. Sensitivity to
843 poly(ADP-ribose) polymerase (PARP) inhibition identifies ubiquitin-specific peptidase 11
844 (USP11) as a regulator of DNA double-strand break repair. *J. Biol. Chem.*
845 doi:10.1074/jbc.M110.104745.

846 Woolhouse, M., and E. Gaunt. 2007. Ecological Origins of Novel Human Pathogens. *Crit. Rev.*
847 *Microbiol.* 33:231–242. doi:10.1080/10408410701647560.

848 Woolhouse, M.E.J., and L. Brierley. 2018. Epidemiological characteristics of human-infective
849 RNA viruses. *Sci. Data*. 5:1–6. doi:10.1038/sdata.2018.17.

850 Yamayoshi, S., G. Neumann, and Y. Kawaoka. 2010. Role of the GTPase Rab1b in Ebolavirus
851 Particle Formation. *J. Virol.* 84:4816–4820. doi:10.1128/jvi.00010-10.

852 Yu, G., L.G. Wang, Y. Han, and Q.Y. He. 2012. ClusterProfiler: An R package for comparing
853 biological themes among gene clusters. *Omi. A J. Integr. Biol.* 16:284–287.
854 doi:10.1089/omi.2011.0118.

855 Zhou, H., M. Xu, Q. Huang, A.T. Gates, X.D. Zhang, J.C. Castle, E. Stec, M. Ferrer, B. Strulovici,
856 D.J. Hazuda, and A.S. Espeseth. 2008. Genome-Scale RNAi Screen for Host Factors
857 Required for HIV Replication. *Cell Host Microbe*. 4:495–504.
858 doi:10.1016/j.chom.2008.10.004.

859 Zotenko, E., J. Mestre, D.P. O'Leary, and T.M. Przytycka. 2008. Why do hubs in the yeast protein
860 interaction network tend to be essential: Reexamining the connection between the network
861 topology and essentiality. *PLoS Comput. Biol.* 4. doi:10.1371/journal.pcbi.1000140.

862

863 **Figure Legends**

864 Figure 1. **Extending the principle of synthetic lethal interactions to a virus-induced**
865 **hypomorph.** (**A**) Synthetic lethality is an extreme negative genetic interaction occurring between
866 two genes. Here, genes 'A' and 'B' are not essential, and the cell remains viable upon the loss of
867 either gene, depicted by red dotted outline of 'A' or 'B', individually. However, when these
868 deletions are combined in a single cell, as visualized in the third panel, this double loss of function
869 critically impairs the cell, resulting in its death. Such gene-gene combinations are termed synthetic
870 lethal (SL) partners. (**B**) The principle of synthetic lethality has been successfully exploited in the
871 development of certain cancer therapies by targeting the synthetic lethal partner of the cancer-
872 causing oncogene, depicted by a red 'A'. In the cancerous cell, gene 'A' has been mutated,
873 depicted as 'A*', leading to an enhanced dependency by the cancer cell for its synthetic lethal
874 partner 'B'. Drugs that target the otherwise nonessential gene B induce cell death when combined
875 with its SL partner, A*. Therefore, inhibiting the function of B can selectively kill cancerous cells
876 while sparing noncancerous bystander cells. (**C**) Like the example in cancer (B), a viral infection
877 provides opportunities for specifically targeting infected cells by synthetic lethality. When a cell is
878 infected, host factors, depicted as the red letter 'A', are recruited by viral proteins to support viral
879 reproduction. The normal function of the host factor is thus attenuated by the presence of the
880 virus, inducing a hypomorph, red letter 'A', which sensitizes the infected cell to inhibition of its
881 synthetic lethal partner by an inhibitory drug.

882 Figure 2. **A chemogenomic screen identifies synthetic lethal partners of GBF1**. (**A**) A
883 schematic of the experimental design for chemogenomic screening with the GBF1 inhibitor
884 golgicide A (GCA). A CRISPR extended knockout (EKO) library of NALM6-Cas9 cells was treated
885 with 2 μg/ml doxycycline to induce individual gene knockouts via Cas9 expression. The pooled
886 library was split into individual flasks and grown over 8 days period in the presence or absence of
887 4 μM golgicide A (GCA). Following incubation, guide RNA frequencies were measured using

888 Illumina sequencing, and $\log_2$ fold changes between GCA and control samples were compared.
889 (**B**) A plot of relative sgRNA frequencies of all genes showing genes passing a 0.05 FDR cutoff
890 in white circles. The 53 genes with negative sgRNA fold change from GCA treatment represent
891 putative synthetic lethal interactors of *GBF1*. The 17 genes with overrepresented sgRNAs and
892 positive sgRNA fold change represent *GBF1* suppressors that may confer protection against
893 GCA. (**C**) Gene ontology functional enrichment analysis of synthetic lethal partners of *GBF1***.** The
894 53 putative synthetic lethal partners of *GBF1* were analyzed in clusterProfiler against the entire
895 KO gene collection from the CRISPR library to functionally classify the SL genes**.** Significantly
896 enriched gene ontologies are plotted and ranked by their $-\log_{10}$, FDR-adjusted enrichment p-
897 value. The number of putative synthetic lethal genes in each gene ontology is coded by the
898 heatmap and ranges from 3 (yellow) to 9 (pink). (**D**) A combined PPI network of the 53 synthetic
899 lethal interactors of *GBF1* (green circles) and the 17 *GBF1* suppressors (orange circles) was
900 obtained from the STRING database and visualized using Cytoscape. Edges between two circles
901 denote evidence-based interaction between the connecting proteins. Circles with red outlines
902 highlight known targets of viral proteins, as per the VirHostNet (v2.0) virus-host PPIs database.
903 Gene names of the proteins and their gene ontology functions are color matched.

904 Figure 3. **Validation of putative synthetic lethal interactions in HeLa cells.** (**A**) *ARF1* displays
905 a robust synthetic lethal interaction with *GBF1*. *ARF1*, *HSP90*, *CSK*, *PRKAA1*, the control gene
906 *MSMO1*, and the top *GBF1* suppressor gene *ARF4* were silenced in HeLa cells with shRNA-
907 mediated lentivirus transductions and incubated with 1.5 or 4 μM golgicide A (GCA) or DMSO for
908 48 h. CellTiterBlue reagent was added and fluorescence measurements were collected. Live cells
909 metabolize the reagent into fluorescent products and an increase in the fluorescence signal is
910 directly proportional to the number of living cells. The percent viability at each GCA concentration
911 was calculated by dividing the fluorescence from a GCA-treated sample by its matched DMSO-
912 treated control. Changes in cell viabilities for each knockdown (KD) cell line were determined by

913 comparing the respective percent viabilities to the *MSMO1* KD control using a Brown Forsythe
914 and Welch ANOVA multiple comparison test (Brown and Forsythe, 1974; Welch, 1951), with
915 statistically significant differences are indicated as: * if *p*-value < 0.01; ** if *p*-value < 0.001; *** if
916 *p*-value <0.0001. Error bars represent the SEM from three biological replicates. (**B**) *ARF1* KD
917 cells show enhanced sensitivity in a GCA dose-response curve**.** A GCA or DMSO working
918 solution (200 μM) was serially diluted and co-plated with 20,000 cells per well of *ARF1* KD and
919 *MSMO1* KD cells in a 96-well plate, with final GCA or DMSO concentrations ranging from 0 – 100
920 μM. After 48 h, cell viability was measured with CellTiterBlue and the normalized fluorescence,
921 relative to the DMSO-treated samples, was calculated using the smallest and largest mean values
922 to define 0% and 100%, respectively. A dose reponse curve of the normalized fluorescence was
923 plotted against the $\log_{10}$ GCA concentration and IC_{50} values were calculated using the a four
924 parameter logistic regression model in Graphpad. Error bars represent the SEM from three
925 biological replicates.

926 Figure 4. **Poliovirus nonstructural protein 3A induces a *vi-hypomorph* of GBF1.** (**A**)
927 Poliovirus 3A physically interacts with GBF1. HeLa cells were transfected with FLAG* tagged
928 poliovirus 3A or an empty control plasmid for 24 h. Equal amounts of lysates were prepared, and
929 immunoaffinity enriched for bound protein complexes to 3A-FLAG* protein. Affinity captured
930 proteins were eluted and resolved on SDS-PAGE along with 1% of the total input lysate and the
931 final wash. Resolved proteins were transferred to a nitrocellulose membrane and immunoblotted
932 using anti-GBF1 (top panel) and anti-FLAG (bottom panel) antibodies. (**B**) Poliovirus 3A
933 redistributes GBF1 away from its perinuclear localization. HeLa cells transfected with FLAG*
934 tagged poliovirus 3A or an empty control plasmid were fixed, stained with fluorescently labeled
935 antibodies against FLAG and GBF1, and imaged by wide-field fluorescence microscopy. Bar 5
936 μM. (**C-D**) Images of GBF1 were analyzed and the distances of each GBF1 puncta to the nearest
937 nucleus was determined and plotted across the entire distance range (C) and between 20 μM to

938 40 μM (D) for 42 control cells and 13 cells transfected with 3A-FLAG*. The corresponding box
939 plots show statistically significant differences in GBF1 distribution between the two samples with
940 *** representing a *p*-value <0.0001.

941 Figure 5. **Synthetic lethal killing of a vi-hypomorph of GBF1.** (**A**) Expression of poliovirus 3A-
942 FLAG* in *ARF1* and *MSMO1*. Each gene was stably silenced in HeLa cells and transfected with
943 FLAG*-tagged poliovirus 3A. The expression levels of 3A-FLAG 48 h post transfection were
944 measured by flow cytometry. (**B**) Poliovirus 3A induces cell death in *ARF1* KD cells. Cell viabilities
945 of *ARF1* KD and *MSMO1* KD cells transfected with 3A-FLAG* or an empty plasmid control were
946 measured using the fluorescence readout of CellTiterBlue. A change in fluorescence is directly
947 proportional to the number of living cells, and a decrease in the absolute fluorescence indicates
948 reduced cell viability. Percent viabilities of ARF1 KD and MSMO1 KD cells were calculated by
949 dividing the absolute fluorescence values of 3A-transfected samples by the matched empty-
950 transfected samples. Multiple t-test was used to compare percent viability between the 3A-treated
951 *ARF1* KD and *MSMO1* KD cells with ****** representing P-value < 0.000001. Error bars represent
952 the SEM from six biological replicates.
953

A *synthetic lethality*

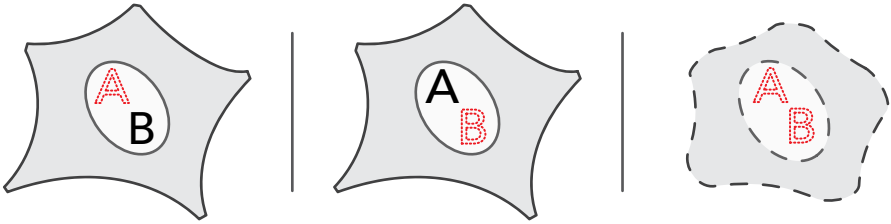

viable viable dead

B *synthetic lethal targeting of cancer*

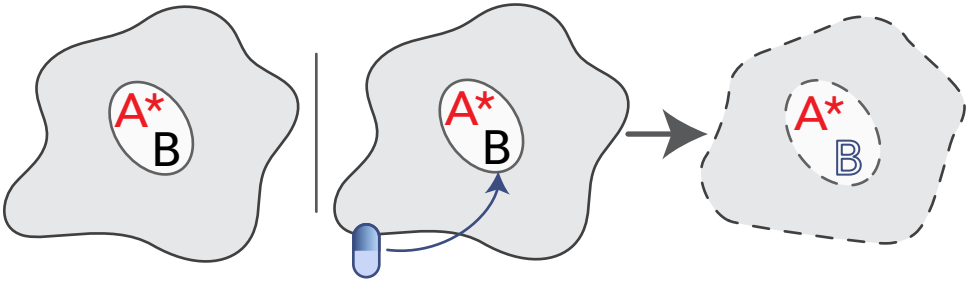

viable drugging SL partner of A* dead

C *synthetic lethal targeting of a viral-induced hypomorph*

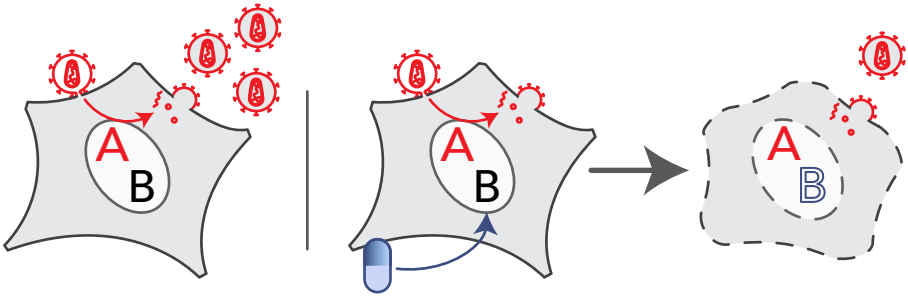

viable drugging SL partner of A dead

Navare et al Figure 1

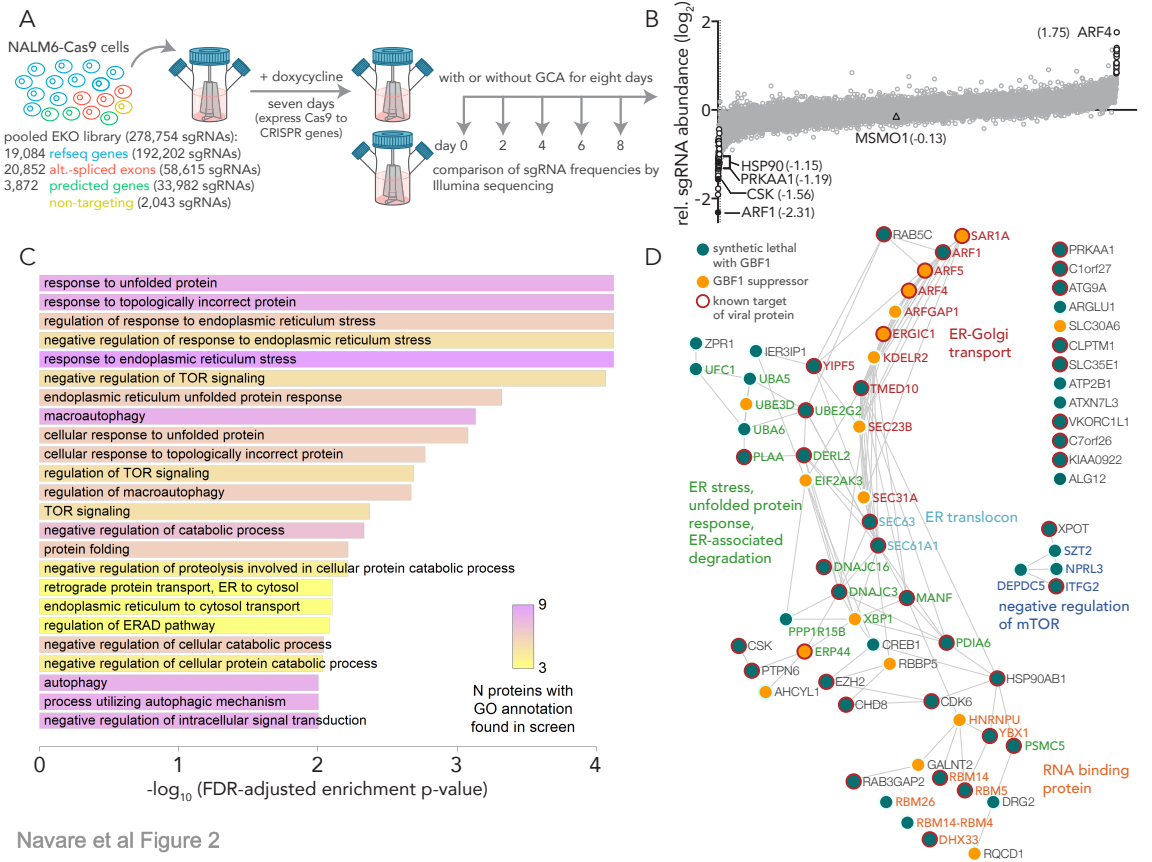

Navare et al Figure 2

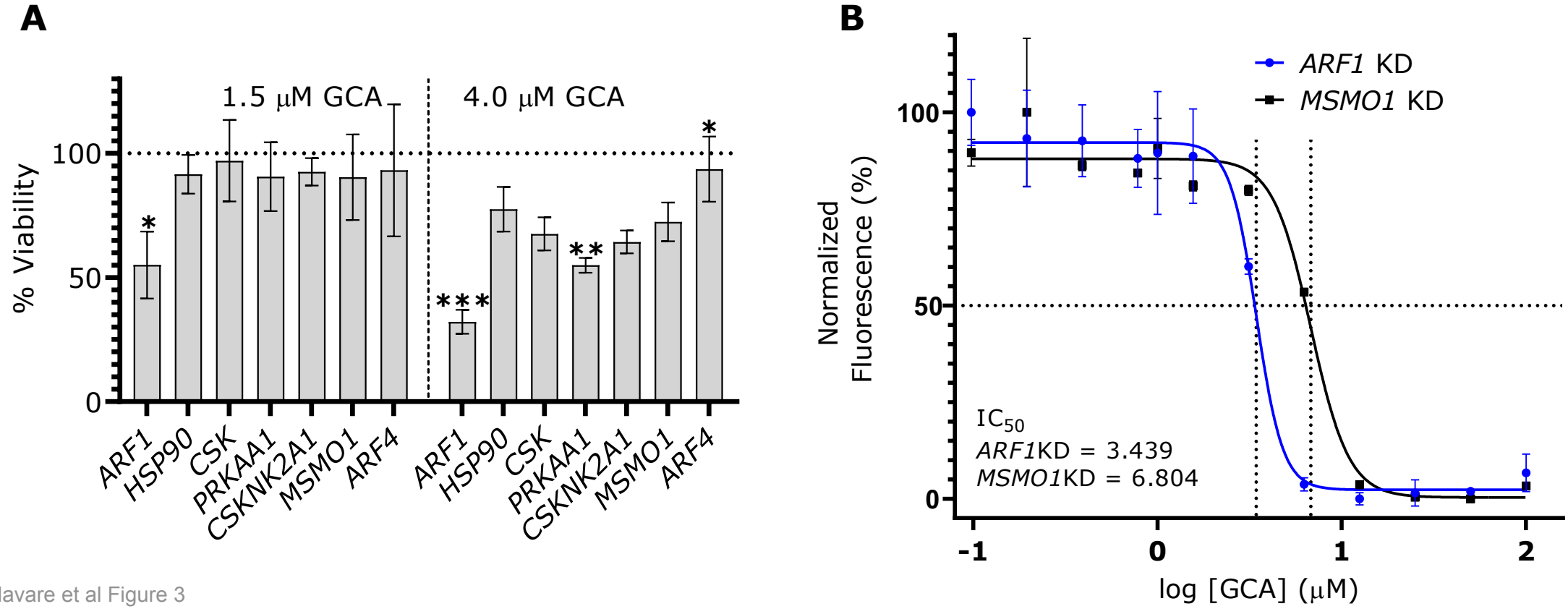

Navare et al Figure 3

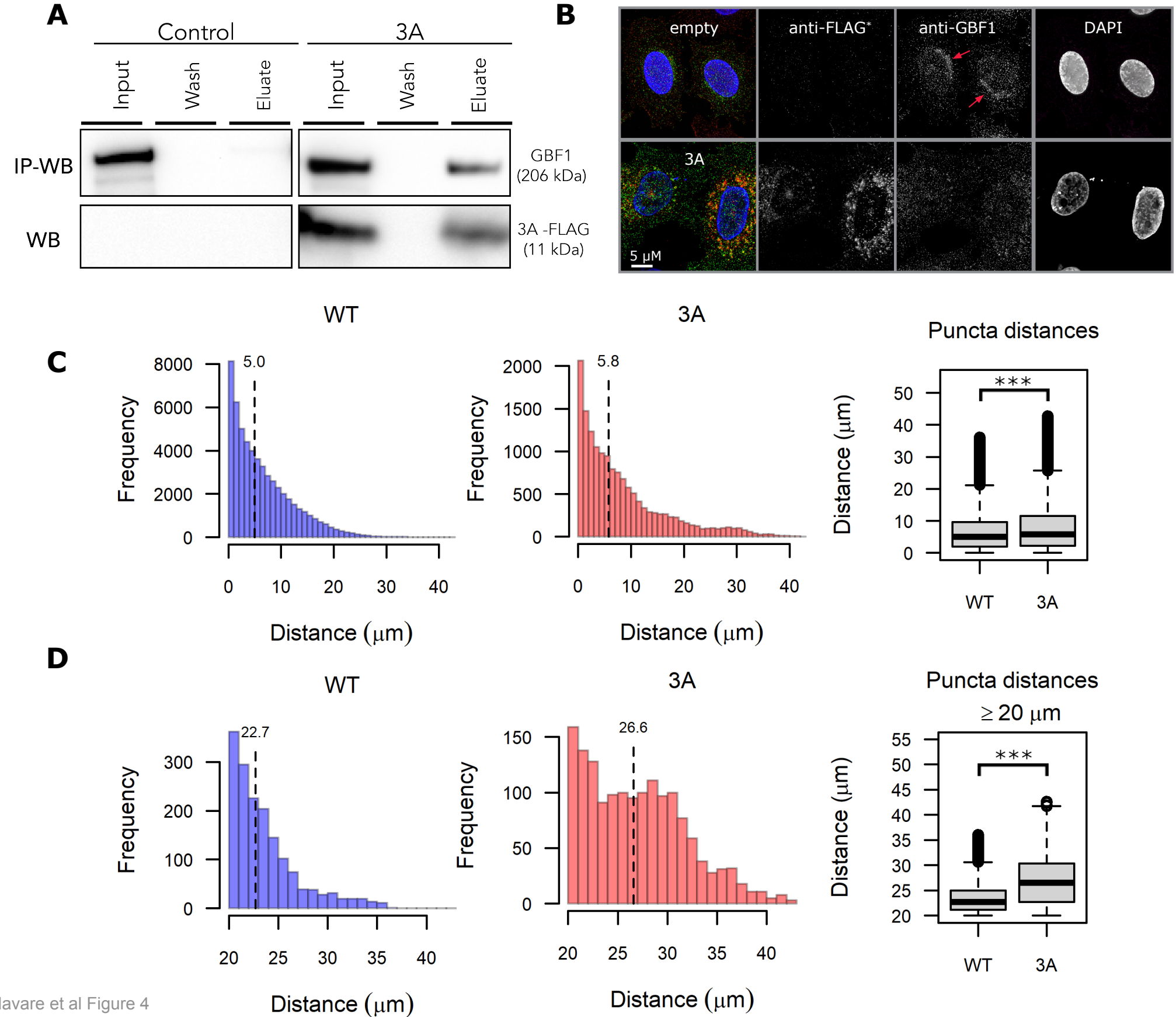

Navare et al Figure 4

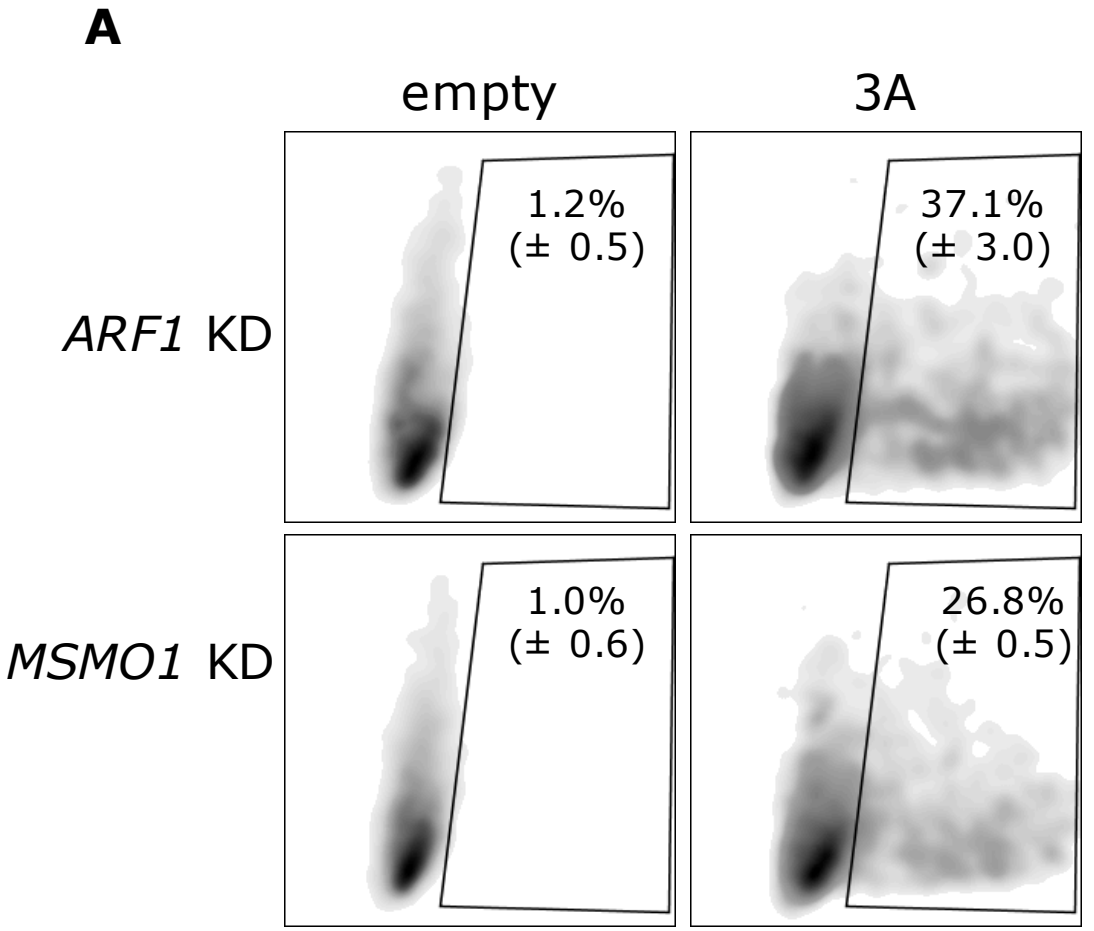

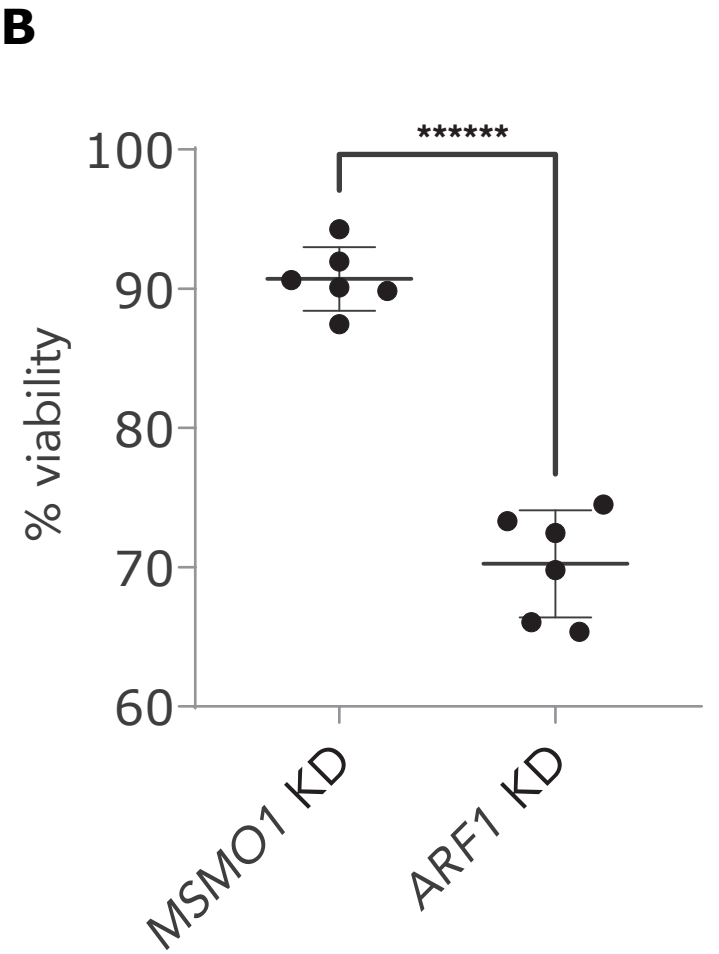

Navare et al Figure 5